A STUDY OF
SINGLE AND POLYCRYSTALLINE INGOT IRON
UNDER REPEATED STRESS

Thesis by

Frank Ambrose McClintock

In Partial Fulfillment of the Requirements

For the Degree of

Doctor of Philosophy

California Institute of Technology

Pasadena, California

1949

To

Mary Whitmore McClintock

Laboratory Technician

Stenographer

Mother

Wife

ACKNOWLEDGEMENTS

This work was carried out in the Dynamics Laboratory of the California Institute of Technology under the supervision of Professor D. E. Hudson, whom the writer thanks for advice and encouragement throughout the program. He also wishes to thank Professor D. S. Clark, Professor P. E. Duwez, and Professor G. W. Housner, who freely contributed their time to discuss problems which arose. Essential metallurgical equipment was made available by Professor Clark and Professor Duwez.

The writer is grateful to the Institute for financial assistance. A generous fellowship awarded by the Shell Oil Company in 1947-8 is also deeply appreciated.

ABSTRACT

Specimens of single and polycrystalline ingot iron were tested in a rotary bending fatigue machine and examined microscopically in order to check previous observations of slip and to study the nature of crack formation and growth. As has been reported, slip takes place on surfaces of high shear stress parallel to a ⟨111⟩ direction in the crystal lattice. In contrast to recent work, the slip was found to occur on wavy surfaces rather than pairs of crystallographic planes.

Fatigue cracks were found to follow surfaces of high shear stress containing a ⟨111⟩ direction. The conclusion that fatigue failures are primarily shear failures is strengthened by a statistical explanation of the mechanism by which a microscopic shear failure can lead to the apparent tension failure commonly observed in rotary bending tests on polycrystalline iron. Microscopic observation of the polycrystalline specimens revealed that cracks originate at the grain boundaries before 30,000 cycles in a specimen which would very probably run for at least 106,000 cycles.

SUMMARY OF CONCLUSIONS

The following conclusions were drawn from rotary bending fatigue tests of single crystals of ingot iron grown by the strain-anneal method:

1. Slip occurred on wavy surfaces of high shear stress parallel to a ⟨111⟩ direction of the crystal lattice.

2. Cracks started from inclusions after several hundred thousand cycles of tensile stresses near 20,000 psi.

3. The cracks occurred on surfaces of high shear stress containing a ⟨111⟩ direction so that a diagonal failure occurred.

4. Cleavage fractures on the (100) plane were found in two exceptional instances.

The following conclusions were drawn from tests of polycrystalline specimens of the same material.

5. Specimens annealed after polishing showed considerable surface deformation and some stress oxidation before failure.

6. Microscopic examination showed that cracks begin in the neighborhood of grain boundaries where the cold work was most severe.

7. At a tensile stress of 27,000 psi these cracks occurred after 7,500 cycles and before 30,000 cycles in specimens whose life would very probably have been no less than 106,000 cycles.

8. As previously found, the cracks grew in a zig-zag manner, usually traversing grains, but occasionally following a boundary.

9. An anneal-polish-run process carried out after every 7,500 cycles at 27,000 psi removed all visible traces of damage, but resulted in excessive grain growth.

10. A statistical analysis explains the mechanism by which a shear failure can result in the apparent tension failure of polycrystalline iron in bending. Fatigue failures may therefore be considered to be shear failures.

11. In fatigue tests on tapered specimens the presence of unknown variables can be detected by comparing the variation in the number of cycles to failure with the variation in the location of failure.

TABLE OF CONTENTS

I: INTRODUCTION

In the middle of the nineteenth century Wohler in Germany and Fairbairn in England showed that metals will fail under repeated applications of a stress below the ultimate strength of the metal and sometimes even below the apparent elastic limit. The failure was caused by the growth of a fine crack during a number of cycles until the cross section was so reduced that rupture followed. This phenomenon, commonly known as the fatigue of metals, is of practical importance because it may cause failures in machine parts after a period of satisfactory service. Furthermore, impending fatigue failures are more difficult to detect than other types such as those due to creep, corrosion, and wear.

A large amount of work has been done on fatigue problems of technical importance. These problems include the number of cycles of stress that can be applied before failure, industrial methods of crack detection, and the effects of such variables as size, surface conditions, steady stresses, combined stresses, varying load cycles, and temperature.

Comparatively few investigations have been made of the mechanism of failure at its earliest stages, particularly on a microscopic scale. The object of the present study is to help fill this gap. Iron was chosen as a material for study for three reasons. Much is already

known about its behavior from previous investigations. It has the interesting characteristic of being able to withstand indefinitely stresses somewhat above the yield point. Finally, it has a relatively simple structure.

Ordinary iron consists of an assembly of many small crystals whose elastic properties vary with their orientation. Therefore, even though a macroscopically uniform stress is applied to the material, there will be microscopic variations in the stress. Some idea of the magnitude of these variations can be obtained from Donnell's work (1) on stress concentrations due to elliptical discontinuities in the stiffness of plates under edge forces. He found that such a discontinuity could cause a stress concentration which was of the order of the ratio of the moduli of elasticity. Since Young's modulus may vary by a factor of two in a single crystal of iron depending on the orientation (2), it is reasonable to assume that the stress concentrations in polycrystalline iron are of this order of magnitude. In order to avoid these stress concentrations and to apply a more nearly known stress, single crystals of iron were grown and tested. Large crystals have the additional advantage that their crystallographic directions can be determined by X-ray methods.

The only previous fatigue test of a single crystal of iron was that made by Gough (3), who tested one iron

crystal in alternating torsion. After gradually increasing the load he found the specimen failed after 118,000 cycles at 16,200 psi shear stress. He found that the cracks spread in the direction of maximum shear stress, regardless of the crystal orientation. Because the specimen was run to failure there was no opportunity to study cracks in their early stages.

On the basis of his fatigue tests, Gough (3) originally found that the slip lines, which are the intersections of the slip surfaces with the specimen surface, varied from straight lines to wavy ones which sometimes appeared to be made up of short segments of two different slopes. Later, however, he proposed that slip occurs on crystallographic planes of the {110}, {112}, or {123} types (4). The particular planes chosen are those immediately on either side of the plane of maximum resolved shear stress containing the slip direction, which is a <111> direction. This hypothesis requires that slip lines consist of two sets of straight line segments, except when the <111> direction lies on the surface of the specimen. In that case, the traces of all those planes coincide and straight lines will be seen.

In static tests, Taylor and Elam (5) also found wavy slip lines and proposed that iron slipped in a <111> direction, but on no particular planes containing that direction. Other investigators (see summary by Barrett, Ansel, and Mehl (6)) have agreed with Gough's or Taylor

and Elam's hypothesis, or have reported that the slip is confined solely to a {123} plane. In every case but one, however, the slip occurred in a <111> direction. In that one case Elam (7) assumed that the slip surface was a plane and found that that plane did not contain a <111> direction. Since the slip surface may not be a plane, and since her observations were made after 8% strain, there may be some question about the result. It is also possible to question the work of Barrett, Ansel, and Mehl (6) who concluded that the slip lines were traces of {110}, {112}, and {123} planes as in Gough's hypothesis. In their work no measurements were made on curved or wavy lines. As a result, their measurements were made in regions where the slip direction lay near the surface. The traces of the various planes containing the slip direction were therefore so close together that traces of several different planes fall within the experimental accuracy of their results.

The present study of single crystal fatigue specimens therefore contributes new information about the fatigue cracks in their early stages, and adds to the controversy about the slip surface of iron.

Polycrystalline tests were made in connection with the single crystal tests as a check on the material and its known behavior. These tests also afforded an opportunity for the microscopic observation of cracks in their early stages.

Microscopic studies of fatigue in polycrystalline ingot iron have been made by Ewing and Humphrey (8), Stanton and Bairstow (9), Gough and Hansen (10), Lucas (11), and Moore and Ver (12). These investigators found what appeared to be dark massed slip lines developing into cracks which usually traversed the crystals but occasionally followed grain boundaries or inclusions. The fact that the fatigue cracks follow the slip lines is contrary to Gough's results for single crystals (4) mentioned above. No special attempt was made to find out how early the cracks formed, although Stanton and Bairstow (9) noticed cracks after 174,000 cycles in a specimen which lasted for 306,000 cycles.

The polycrystalline part of the present study therefore contributes to the knowledge of how soon cracks form and what governs their direction of growth.

II: EXPERIMENTAL TECHNIQUE

Material

Round specimens were chosen for testing in order that a suitable polish and a known geometry could be obtained over the entire section in which failure was likely to occur. Microscopic observation at 400X requires a specimen with a minimum radius of curvature of the order of .1 in. Ingot iron was chosen for the experimental material because it was readily available in the size and quantity desired, and because it would have required two to three weeks to decarburize a low carbon steel (13).

A number of 11/16 in. cold rolled bars were bought simultaneously. Cut-off markings were similar, but there was no proof that they came from the same heat. The bars were denoted by Roman numerals. The blanks cut from each bar were given the corresponding Roman numeral and an Arabic numeral. Alternate blanks were assigned to single and polycrystalline tests, except for Bar III, all of which was used for crystal growth.

A chemical analysis of four different bars indicated no significant differences. The average results follow:

Carbon	.02%
Manganese	.03%
Phosphorus	.01%
Sulphur	.03%
Silicon	.001%
Oxygen (Bar V only)	.07%

Tensile tests of this material after an anneal at 1700 F followed by cooling at 100 F/ hr showed a lower yield point of 16,000 psi, an ultimate strength of 42,000 psi, and a 70% reduction of area.

Single Crystal Fatigue Specimens

The blanks for crystal growth were machined into tensile test specimens with threaded ends before annealing. The center section was .384 in. diameter by 1 9/16 in. long with 1/8 in. fillets to the .505 in. diameter shoulder. After annealing they were strained 3 to 4% in tension and annealed in a hydrogen atmosphere for a few days to a week at temperatures of about 1640 F, just below the α-γ transformation in iron. In some cases single crystals grew over practically the entire test section. These single crystals were often marred by the presence of crystallites of the order of .01 in. diameter. The long anneal required for crystal growth resulted in weak grain boundaries due to the presence of inclusions, probably oxides. Details of the crystal growth and the grain boundary weakness are given in Appendices I and II.

As a result of the grain boundary weakness, no specimens could be tested which had a transverse joint between two large crystals in the center of the specimen. In order to insure that failure would not occur where the single crystal joined the polycrystalline material at the ends, the

center section was turned down to a .22 in. diameter with a 4.68 in. radius of curvature in the longitudinal direction. Thus the nominal stress at the joint was about one eighth of the maximum stress in the test section.

After being machined the specimens were polished and etched until no traces of cold work due to machining were visible. When a sharp-nosed tool was used in machining the cold work extended only about 0.001 in. below the surface. When a 1/8 in. radius tool was used, however, the cold work was found to extend several times as far. The final polishing consisted of a circumferential polish with wet 400 grit Aloxite paper. This was alternated with a 20 second etch in a 3% solution of nitric acid in methanol. The time required for polishing these specimens was ten to twenty times that required by metallurgical specimens of the same material, polished with the same paper. One reason for this difference is that due to the compound curvature of the fatigue specimen surface, only a small fraction of the area was being polished at any one instant, whereas in polishing a flat specimen on a plate all the specimen is being polished all the time that the two are in contact. An electrolytic polish would have been desirable, but the marked presence of inclusions in the ingot iron caused excessive pitting when much material was polished off.

The orientation of the crystal lattice in the specimens was determined with X-rays as described in Appendix III.

A rotary bending fatigue test was chosen because it had been commonly used for polycrystalline material and because no single crystal work had been done with it. As shown in Appendix IV, the anisotropy of the single crystal will cause no trouble as long as the crystal remains elastic. Gough thought that once slip occurred, the unsymmetrical nature of the slip would cause distortion (4). He had previously found that large deformations occurred in an alternating axial load machine. In that case, however, the tension load decreases the cross-sectional area and raises the stress, whereas the compression load increases the area and decreases the stress. This leads to progressive elongation of the specimen even under alternating loads of equal magnitude. No such effect was expected in the reversed bending test. That is, if slip occurred in one direction in one part of a cycle, no reason was seen why compensating slip should not occur in the other half of the cycle so that no serious overall deformations would result. No difficulty was encountered in these tests except in the test at the highest stress when a marked distortion of the specimen did occur.

Polycrystalline Fatigue Specimens

Blanks for the polycrystalline specimens were annealed in lots of twenty-five or thirty in an electric hearth furnace open to the atmosphere. They were heated to 1700 F for a half hour and then furnace cooled at an

Fig. 1

Rotary Bending Fatigue Machine

and Accessories

initial cooling rate of about 450°F/hr. The resulting grain size was about 100 grains/mm^2 or ASTM #3½. The specimens were machined to the standard Moore-type test section, .3 in. diameter with a 9 7/8 in. radius of curvature in the longitudinal direction. The specimens were then polished, the last operation being a longitudinal polish with wet 320 grit Aloxite paper. Carrying the polishing process further to a 400 grit paper required an extra two to four hours per specimen and was considered impractical.

Fatigue Machine

The rotary bending fatigue machine and its accessories are shown in Fig. 1. A 1/3 horse power electric motor mounted underneath drove the left-hand spindle through a V-belt and also drove the oil pump for the journal bearings. The bending moment which the bearings would otherwise apply to the specimen could be counter-balanced by the spring-mounted counter-weight shown at the far right. The amplitude due to misalignment was measured by holding a Consolidated Engineering Type 110-B vibration meter where shown.

The running time was measured by a clock connected in parallel with the motor. The motor and clock both stopped when the bearings fell far enough so that an adjustable stop opened a microswitch which in turn opened a holding relay. This prevented the restarting of the machine in the event

of current failure. The speed of rotation was measured with a General Radio Type 631-B Strobotac calibrated against line frequency near the speed of operation. The Strobotac was also used for observing surface deformations during the tests. When the machine was run near 400/rpm, the Westinghouse PSE-2 Stroboglow unit and contactor were used for observation. Also shown on the lower shelf are the tools for changing specimens. The dial on the right hand end of the outboard bearing served to determine the angular coordinates of points on the specimen. The microscope and angular coordinate dial were removed while the specimen was running.

The microscope and camera were mounted on a bar which pivoted about a point 9 7/8 in. from the surface of the specimen. Hence the standard Moore type fatigue specimen could be examined with only minor adjustments in focus. The bar carried a nut which was traversed by a lead screw having twenty threads per inch. The right hand end of this lead screw carried another dial to give readings of the longitudinal coordinate. The center of the specimen was chosen as the origin of the longitudinal coordinate. With a 16 mm objective and 10X eyepiece, the field of view was large enough so that circumferential strips 0.05 in. wide (one turn of the traversing screw) could be examined. Magnifications of 88X and 380X were obtained with the camera using 16 mm and 4 mm objectives with the 10X eyepiece. Using a twenty-one candle-power light and prism

illumination, exposure times of about 15 seconds were found satisfactory for commercial ortho film.

The load imposed by the machine on the specimen was almost entirely bending. The initial load due to the housing, oil, the bearing journals, the specimen, the weight pan and its spring support, but not including dashpots is 28.2 ± 0.2 in.-lb. The moment arm is 6.34 ± 0.03 in. For a 0.300 in. diameter specimen the resulting initial bending stress is 10,600 psi. The bending stress per pound weight in the pan is 1196 psi.

In addition to the bending moment some torque was applied due to bearing friction and vibration of the V-belt drive. The running friction torque was less than 200 psi and torque due to belt vibration was only around 30 psi. The starting torque was measured by wrapping a thread helically around the rubber coupling and fastening it lightly with plasticene. Torsional deflection of the coupling on starting loosened the thread. The amount of slack indicated that the starting torque was no higher than the running torque. The diameters of the specimens were measured with a dial guage to about ±0.0002 in. This error was the principal possible source of scatter in the data aside from the vibration discussed below. It corresponds to a stress variation of 0.2% or a variation in cycles to failure of about 3%.

As originally built, the fatigue machine was equipped with dashpots stiff enough to damp out any vertical

oscillations due to misalignment of the specimen. Mounting of the bearings in trunnions prevented horizontal oscillations. Even with a ground taper on the specimens, the run-out of the assembled machine amounted to as much as 0.003 in. at the inner end of the bearings. The stress resulting from straightening out a specimen by this amount is of the order of 2500 psi. While this stress is a steady one, it was considered high enough to affect the results. The restraint due to the dashpots would have imposed a compression stress on the high side and tension stress on the low side at points of the specimen already under stress due to the bending load. The restraint due to the trunnions was not so serious, for as the high point passed the trunnions, the stress due to straightening was superimposed on a zero stress due to the load. With the dashpots removed and with the loading pan and counter-weights isolated by very soft springs, the bearings and specimen behaved as a single degree of freedom system with an oscillating support. The ratio of the actual stress, τ , to the stress required to straighten, τ_o , is given by

$$\frac{\tau}{\tau_o} = \frac{1}{\frac{\omega_c^2}{\omega^2} - 1}$$

where ω_c is the critical frequency and ω is the operating frequency. Table 1 gives the frequencies and stresses for both the standard Moore-type specimens and the smaller

Table 1

	Poly-crystal	Single Crystal
Specimen diameter, in.	0.300	0.218
Longitudinal radius of curvature, in.	9.88	4.68
Stress required to straighten a runout of 0.001 in. peak to peak, psi	850	1000
Natural frequency, cps	27	18
Frequency operated, cps	13.2	6.8
Stress due to a 0.001 in. peak to peak amplitude, psi	200	160

specimens used in testing the single crystals. Since the misalignment was usually less than 0.003 in. peak-to-peak, the stresses due to misalignment which were superimposed on the bending stresses were usually less than 500 psi. Experimental results indicated no correlation between the vibration and the cycles to failure.

The vibration of the bearings decayed rapidly in the first part of any polycrystalline tests, dropping to a tenth of its original value at 10 to 20 % of the total life at 27,000 psi. If the machine were running below its critical speed and not restrained in any way, the forces acting on the specimen would tend to increase the amplitude of vibration. The fact that the vibration decayed indicates that the restraint of the bearings in

the horizontal direction was enough to straighten out the specimen. The specimen must have had a low enough limit of elasticity so that the stress of 2,500 psi due to straightening out the specimen twice each cycle was enough to produce a slight permanent set. This loss in elasticity would be expected from locked-in stresses due to cold work. If the machine were run above the critical speed, even without bearing restraint, the phase relations would be such that again the forces would reduce the vibration.

After the period of initial decay the vibration remained very small until 90 to 95% of the life had elapsed, at which time it usually increased rapidly. The fatigue machine was set to cut out as soon as the bearing deflection had increased by about 1/32 in. so that the specimen had not broken in two when the test ended. A few tests indicated that only another 2 or 3% of life would be required for complete failure.

Method of Determining Homogeneity in Fatigue Tests

The fatigue machine applies a uniform bending load to a specimen whose thickness varies in the axial direction. Therefore the stress varies along the specimen and if the material were perfectly uniform, failure would occur at the center of the specimen where the stress is a maximum. Failure occasionally occurs elsewhere so there must be local variations in the strength of the material which

can be estimated from the variation in the location of failure. The local variations should also cause a variation in the life of similar specimens tested at the same stress. This variation in life can be calculated from the estimated local variation in strength. If the observed variation in life of a number of apparently identical tests is greater than this calculated value, then the tests are probably not homogeneous. The following analysis develops this method of checking for homogeneity in a quantitative manner.

Let a Moore-type specimen be sub-divided symmetrically into equal segments as shown in Fig. 2. Segments equi-

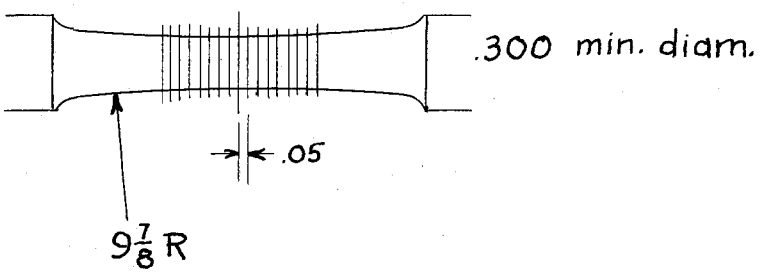

Fig. 2

distant from the center of the specimen are given the same number and will henceforth be considered as one segment.

Assume that if the j^{th} segment were tested alone, the relation between the stress, τ_j , and the cycles to failure, c, is given by

$$\tau_j + K \log c = x_j \quad , \qquad (1)$$

where k is a constant and x_j is a statistical variable, normally distributed with mean m and standard deviation σ. The assumption of a linear relation between log c and τ_j is well justified by experience; the normality assumption is convenient and will be discussed later.

Now let τ_m be the maximum stress in the specimen and define

$$X = \frac{\tau_m + k \log c - m}{\sigma} . \qquad (2)$$

Then $X + \frac{\tau_j - \tau_m}{\sigma}$ is normally distributed with zero mean and unit variance. The probability that the j^{th} segment will fail before the cycles corresponding to x is given by

$$p_j(X) = \frac{1}{\sqrt{2\pi}} \int_{-\infty}^{X} \exp - \frac{\left(x + \frac{\tau_j - \tau_m}{\sigma}\right)^2}{2} \, dx . \qquad (3)$$

The specimen will fail in the j^{th} segment between the cycles corresponding to x and $x + dx$ if it has not failed in any of the other segments previously, and if the j^{th} segment would fail at that time if tested alone. The probability that the specimen will not have failed earlier in another segment, say the i^{th}, is $1 - p_i(x)$. If the probability of failure in one segment tested alone is assumed independent of the probabilities of failure in the other segments, then the probability of getting no failure

TABLE 2

Distribution of $P_j(x)$

$\frac{\tau_m}{\sigma} = 9.64$

x \ j	(1)	(2)	(3)	(4)	(5)	(6)	$\sum_j P_j(x)$
- 4.0	.0001	.0001					.0002
- 3.5	.0008	.0004	.0001				.0013
- 3.0	.0042	.0022	.0006	.0001			.0071
- 2.5	.0166	.0098	.0033	.0005			.0302
- 2.0	.0509	.0329	.0131	.0026	.0002		.0997
- 1.5	.1177	.0832	.0392	.0102	.0010		.2513
- 1.0	.1955	.1487	.0826	.0274	.0037	.0001	.4580
- .5	.2173	.1757	.1098	.0506	.0089	.0005	.5628
0	.1448	.1222	.0846	.0427	.0115	.0010	.4068
.5	.0512	.0446	.0334	.0196	.0069	.0010	.1567
1.0	.0084	.0075	.0060	.0039	.0017	.0004	.0279
1.5	.0006	.0005	.0004	.0003	.0002		.0020
$\int_{-\infty}^{\infty} P_j(x)dx$	.4040	.3139	.1866	.0790	.0170	.0015	1.0020

in any segment other than the j^{th} and getting a failure in the j^{th} is given by the products of the separate probabilities:

$$P_j(x)\,dx = \frac{\prod_{i=1}^{N}\left(1-P_i(x)\right)}{\left(1-P_j(x)\right)}\,\frac{1}{\sqrt{2\pi}}\,\exp-\frac{\left(x+\frac{\tau_j-\tau_m}{\sigma}\right)^2}{2}\,dx. \qquad (4)$$

In order to calculate $P_j(x)$, values for $\frac{\tau_j}{\tau_m}$ and $\frac{\tau_m}{\sigma}$ were chosen. For the standard Moore-type specimen with a 0.3 in. minimum diameter and 9 7/8 in. radius, divided into segments 0.05 in. long on either side of the center, the stress at the center of the j^{th} segment is given approximately by

$$\tau_j = \tau_m\left(1-(0.05j-0.025)^2\right). \qquad (5)$$

Three values were chosen for $\frac{\tau_m}{\sigma}$: 19.27, 9.64, and 1.927. With these assumptions $P_j(x)$ was calculated. The results for $\frac{\tau_m}{\sigma} = 9.64$ are presented in Table 2.

The standard deviations of the marginal distributions were converted to variations in stress and cycles by taking τ_m as 27,000 psi and k as 5500 psi/$\log_{10}(c)$. The latter value was obtained from the work of Moore and Kommers (14). Experimental results from three polycrystalline specimens from each of Bars V, VI, VIII, and IX tested at 27,000 psi and 794 rpm are compared with the theoretical results in

TABLE 3

Comparison of Experimental and Theoretical Variation in Failures

	Theoretical			Experimental*
$\frac{\tau_m}{\sigma}$	19.27	9.64	1.927	
Standard deviation of position of failures, in.	0.128	0.091	0.045	0.024 to 0.066
Standard deviation of $\log_{10}$ (cycles)	0.1840	0.0908	0.0216	0.075 to 0.214 (0.041 to 0.124)
Stress change one standard deviation from the center, psi.	440	225	53	16 to 120
Stress difference required to change the mean of $\log_{10}$ (cycles) by one standard deviation, psi.	1010	500	120	410 to 1200 (230 to 680)

* 98% confidence limits assuming a normal distribution of position and $\log_{10}$ (cycles) respectively. That is, the statistical methods used to set the limits are correct 98% of the time, if the assumption of normality is valid.

Table 3. The figures in parentheses under the heading "Experimental" are those obtained omitting Specimen VI-9, the most extreme experimental point. The theoretical results indicate that the stress change one standard deviation from the center is about half of the strength difference required to change the $\log_{10}$ (cycles) by one standard deviation, regardless of the original assumption for $\frac{\tau_m}{\sigma}$. Since the variation in life is greater than that expected from the variation in failure location, there is probably some factor affecting the lives of the individual specimens other than local variations in the strength of the material. The observed scatter of failure location indicates one should expect a scatter in cycles to failure of only about 2% to 10%. While these figures seem remarkably low, later tests with a different specimen preparation indicated that the scatter in cycles to failure can be reduced to that amount. These results will be further discussed in chapter IV, Polycrystalline Fatigue Tests.

It appears likely therefore, that an experimenter can check his technique by observing the scatter in location of failures and in cycles to failure of supposedly homogeneous tests. If the stress variation due to the former is much more than half the strength variation corresponding to the latter, then the tests probably were not homogeneous.

The assumptions will now be reexamined in the light

of the results obtained. The choice of $\frac{\tau_m}{\sigma}$ is relatively unimportant if one wishes to compare the variation in life with that in location. The assumption that the τ-log c curve is a straight line is, of course, invalid near the endurance limit, but satisfactory elsewhere. The 0.05 in. segment thickness used in this analysis was chosen simply for ease of computation. A smaller segment would reduce the mean of log (cycles) and accentuate the negative skewness of its distribution, as Epstein (15) has shown for a similar case. The assumption of normality is open to serious question, for it results in this negative skewness. It can be shown by applying a χ^2 test to the data of Mueller-Stock given by Batelle (16), that the distribution of log (cycles) is definitely not normal, but skewed positively. Therefore the segments would not have strengths normally distributed if tested alone. But since the results of this analysis are standard deviations, the shape of the distribution is probably not of critical importance.

This method of checking for homogeneity should therefore be useful as a guide to anyone striving for a high degree of accuracy in fatigue tests.

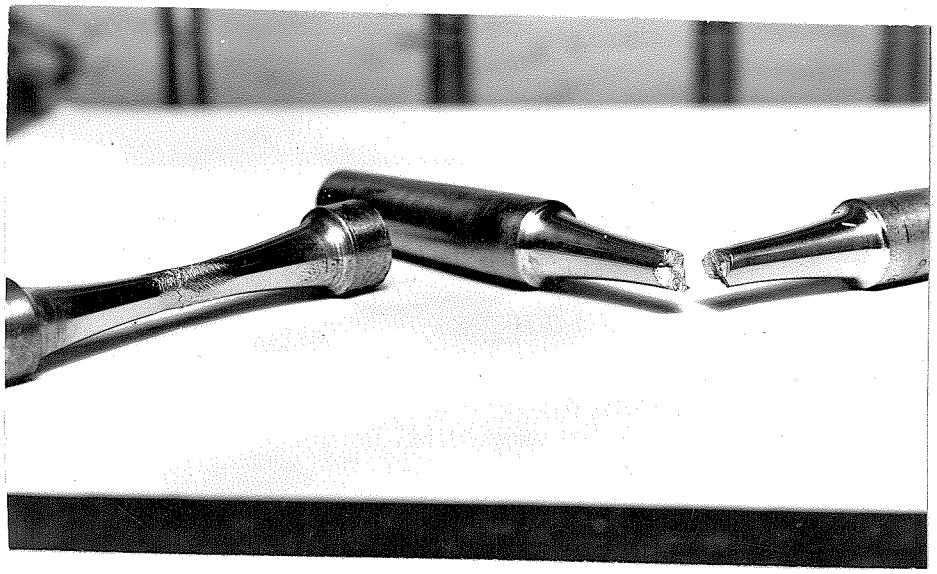

Fig. 3 1X

IV-16
31,500 psi for
11,200 cycles

V-16
20,000 psi for 381,000 cycles
22,100 psi for 166,200 cycles

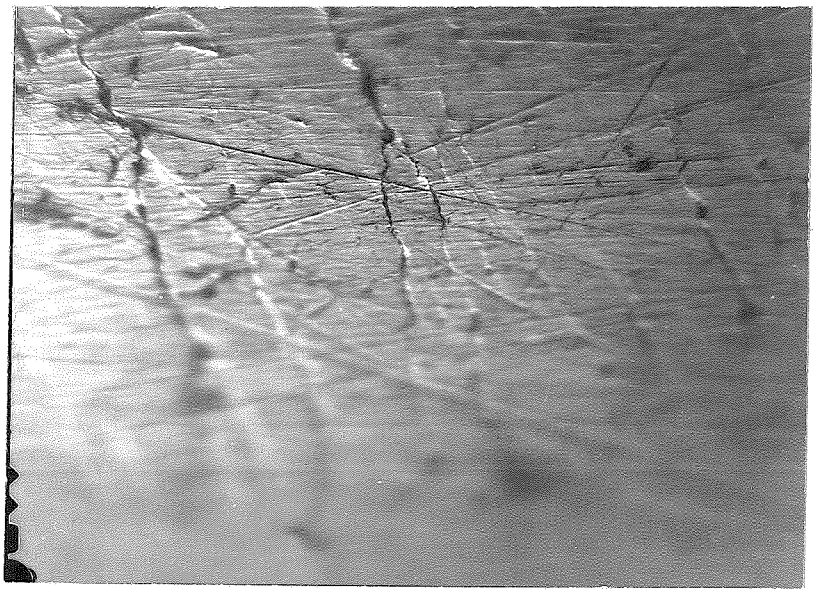

Fig. 4 380X

IV-16 31,500 psi for 11,200 cycles
(local stress nominally 22,500 psi)
S_3 = 0.41 in. ϕ = -95°

III: SINGLE CRYSTAL FATIGUE TESTS

The primary object of the single crystal fatigue tests was to relate the slip lines and cracks to the crystallographic directions. A discussion of these results will be given specimen by specimen.

Specimen IV-16

This specimen was a single crystal with a few 0.01 in. crystallites. The surface was finished with a criss-cross polish. The specimen was run at the lightest stress possible without putting counter weights on the machine, 31,500 psi. Vibration was severe, and caused the machine to stop after 200 cycles. The cut-off switch was backed off and the machine restarted. In the next 1260 cycles the peak-to-peak amplitude of machine vibration decreased from 0.015 in. to 0.004 in. After a total of 5460 cycles a frosty surface appeared and the amplitude had increased to 0.009 in. When the machine stopped after 11,200 cycles, cracks were not visible to the naked eye, but they were opened up by another twenty cycles.

As viewed in Fig. 3, the slip markings on top were concave to the left, while those in front sloped downward to the right. Thus at least two different slip surfaces were active. The cross section had markedly changed shape and the deformations in the center were so great that no attempt was made to analyze the slip and crack directions.

It was noted, however, that the fatigue cracks followed the slip markings in steps. Fig. 4 shows a region off to one side, where the stress was nominally 22,500 psi. S_3 is the axial coordinate measured from the center of the specimen to the center of the figure; ϕ is the angular coordinate from an arbitrary reference mark on the shoulder. In some places the markings appeared to be continuous waves on the surface and in other places appeared to be actual breaks so that the slip surface was visible. One hardly knows whether or not to call these markings cracks. An X-ray diffraction pattern of this region showed no change in spot intensities or diameters. This result is further indication that fatigue damage at low stresses is so local that X-ray methods are of little help.

Specimen V-16

There were a few 0.01 in. crystallites in the surface of this specimen. The polar coordinates of the specimen axis relative to the [100] direction were $\theta = 26.6^\circ$, $\phi = 99.0^\circ$; those of the radius through the reference mark were $\theta = 68.7^\circ$, $\phi = 240.8^\circ$. After 381,000 cycles at 20,400 psi no change had occurred in the vibration of the machine, so the specimen was still somewhat elastic. The load was increased 10% without stopping the machine. After a further 89,400 cycles it was possible to see a crack in the surface using the Stroboglow light. The machine was then stopped and the specimen examined. The original etching had attacked the crystal preferentially and slip lines were practically invisible at the point where slip on

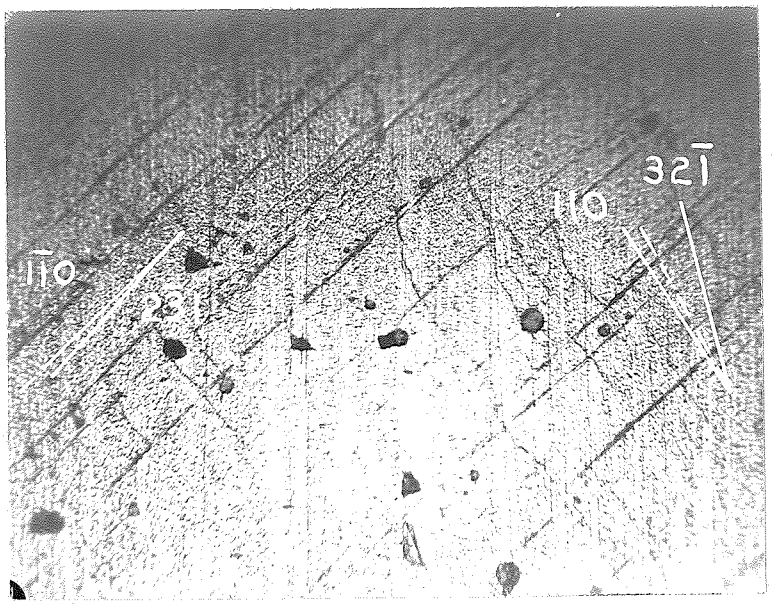

Fig. 5 380X

V-16 20,000 psi for 381,000 cycles
22,100 psi for 89,400 cycles
$S_3 = -0.016$ in. $\phi = 246\frac{1}{2}^{o}$

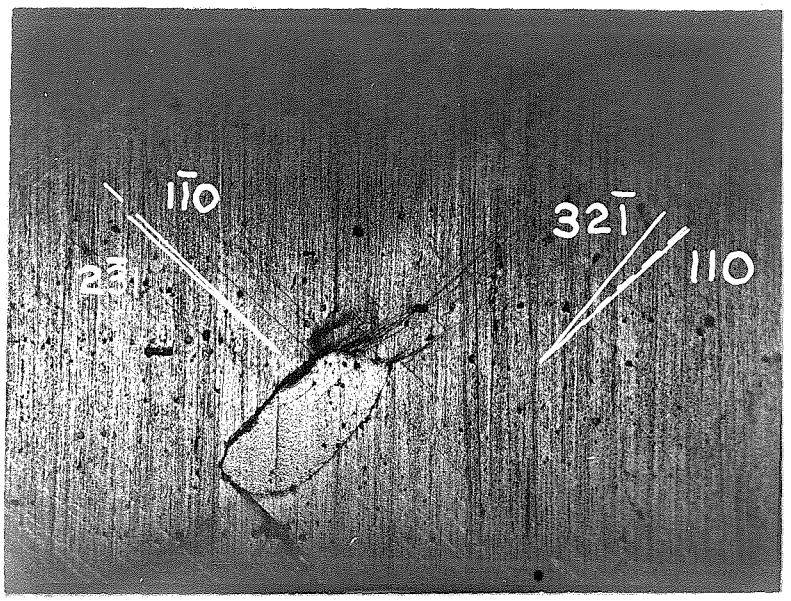

Fig. 6 88X

V-16 20,000 psi for 381,000 cycles
22,100 psi for 89,400 cycles
S_3 = 0.058 in. $\phi = 43^\circ$

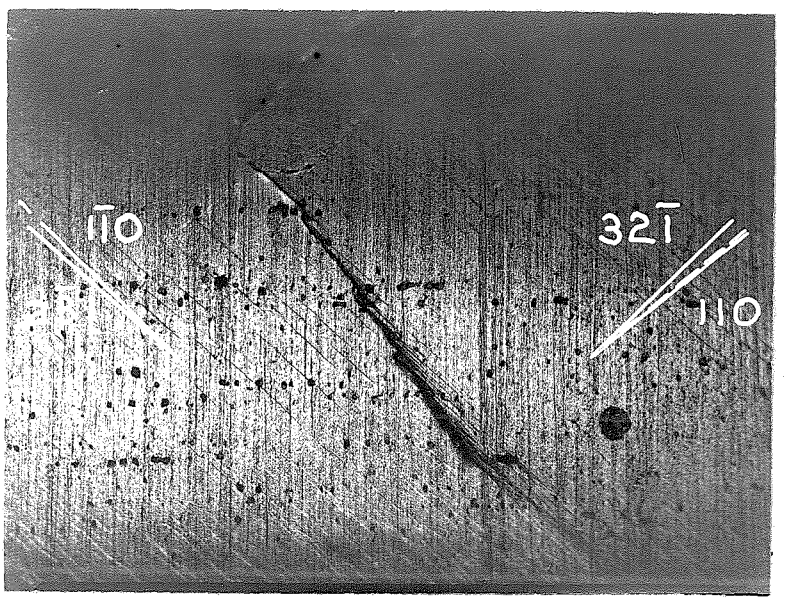

Fig. 7 88X

V-16 20,000 psi for 381,000 cycles
22,100 psi for 89,400 cycles
S_3 = 0.058 in. $\phi = 32\frac{1}{2}^\circ$

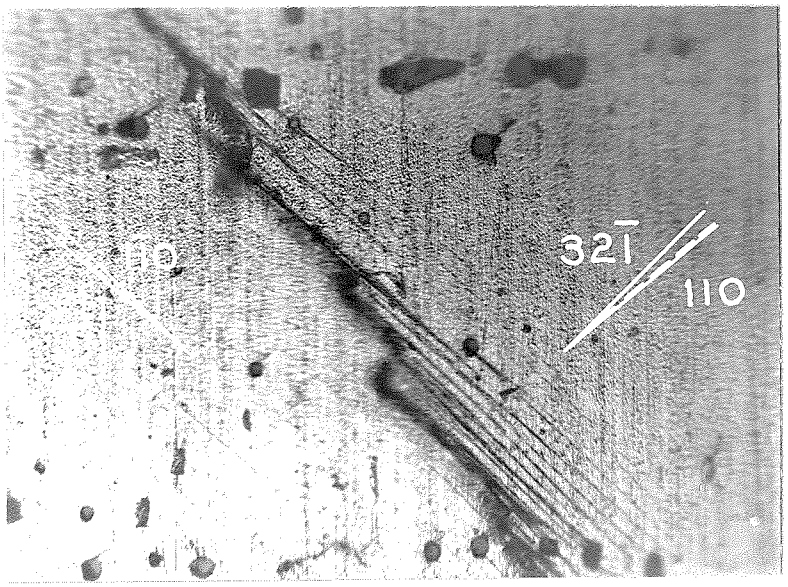

Fig. 8 380X

V-16 20,000 psi for 381,000 cycles
22,100 psi for 89,400 cycles

S_3 = 0.058 in. ϕ = 31°

different planes in the [111] direction would give maximum differences between the lines due to those planes. The slip lines were straight and agreed with the [111] direction where that direction was nearly parallel to the surfaces, as has been reported by previous investigators. At the region shown in Fig. 5 evidence of slip in two different ⟨111⟩ directions was found and in this case the surface had been etched enough so that the character of the slip surface could be distinguished. The maximum resolved shear on a plane containing the $[1\bar{1}1]$ direction (wavy lines) was 94.7% of that on a plane containing the [111] direction (straight lines). Fig. 5 also shows the traces of the crystallographic planes suggested by Gough (4) and traces of the plane of maximum resolved shear stress containing the ⟨111⟩ directions (dotted lines). These traces, determined from X-ray diffraction patterns, are accurate to 1 or 2°. While the $(1\bar{1}0)$ trace seems to follow one set of slip lines quite well, the other set is made up of very irregular lines. If these lines are in fact made up of short segments of traces of the crystallographic planes, the segments cannot be any longer than about 2 mm at this magnification, or 4 microns. They are certainly not the result of intersections of two independent straight slip traces. In another part of the specimen, slip lines similar to those shown by Barrett ((17) p. 292) were found.

Views of the principal crack and the crystallite from which it started are shown in Figs. 6 and 7. Fig. 8 shows

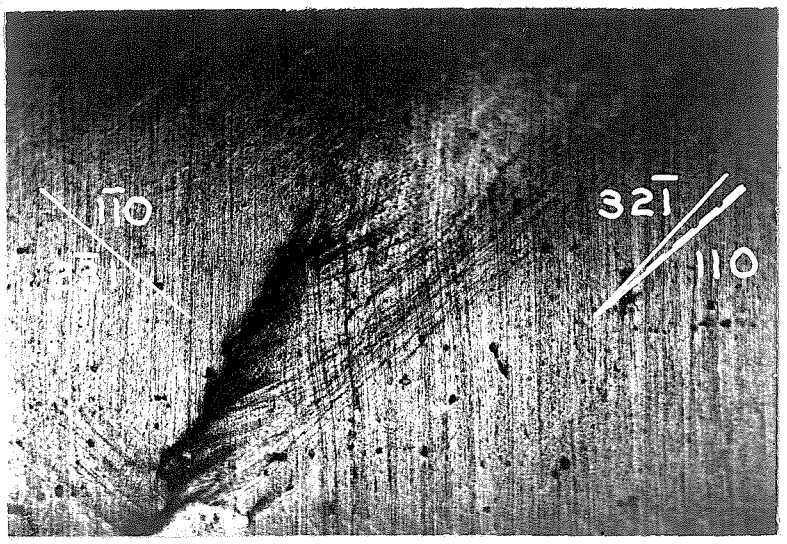

Fig. 9 88X

V-16 20,000 psi for 381,000 cycles
22,100 psi for 131,000 cycles
S_3 = 0.086 in. $\phi = 47\frac{1}{2}^{o}$

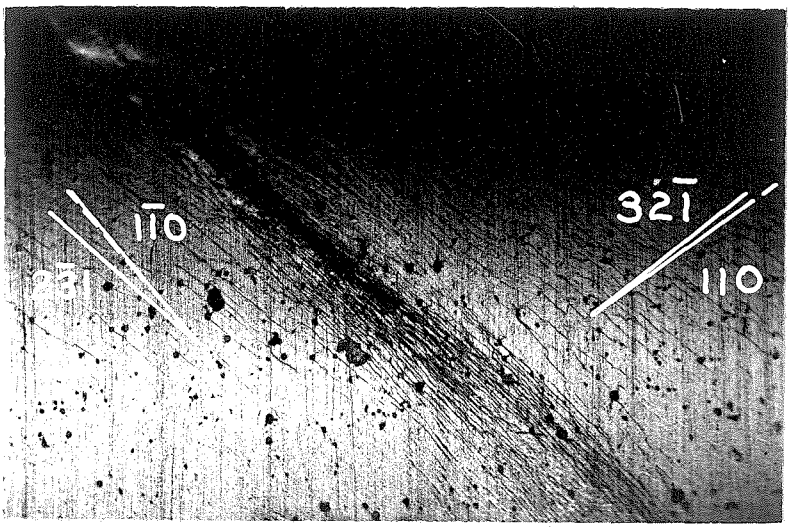

Fig. 10 88X

V-16 20,000 psi for 381,000 cycles
22,100 psi for 131,000 cycles
S_3 = 0.026 in. $\phi = 13^{o}$

Fig. 11 88X

V-16 20,000 psi for 381,000 cycles
22,100 psi for 89,400 cycles
S_3 = -0.043 in. $\phi = 315\frac{1}{2}^{o}$

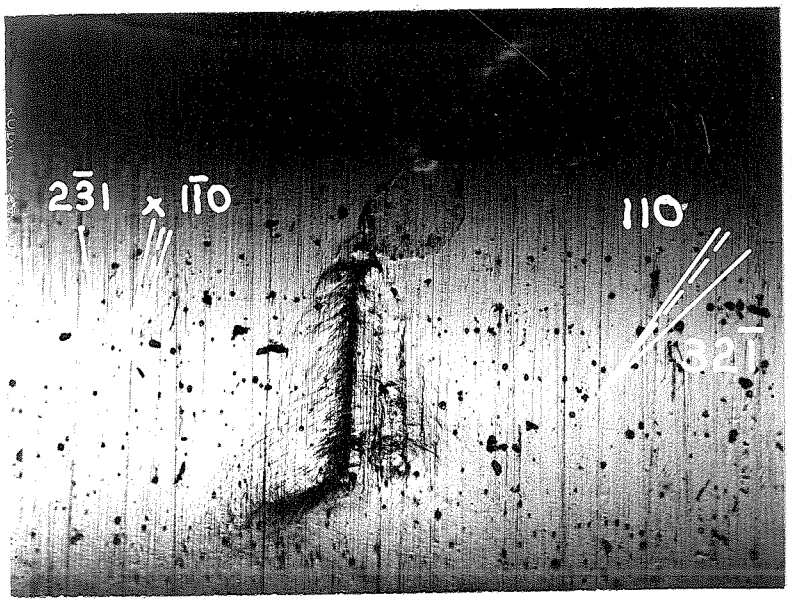

Fig. 12 88X

V-16 20,000 psi for 381,000 cycles
22,100 psi for 89,400 cycles
S_3 = -0.045 in. $\phi = 305^{o}$

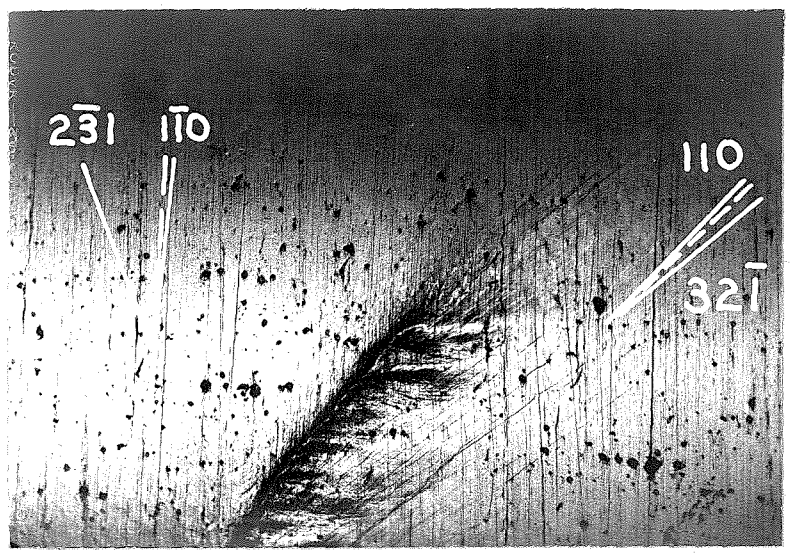

Fig.13 88X

V-16 20,000 psi for 381,000 cycles
22,000 psi for 131,900 cycles
S_3 = -0.070 in. ϕ = 317°

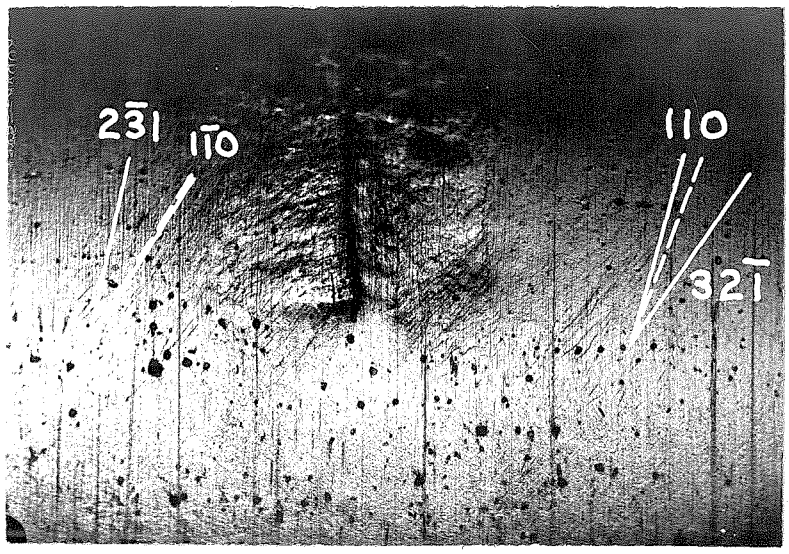

Fig. 14 88X

V-16 20,000 psi for 381,000 cycles
22,000 psi for 131,900 cycles
S_3 = -0.050 in. ϕ = 286°

TABLE 4

Crack Lengths in Specimen V-16, Inches

Figure No.	6, 9	7, 10	11, 13	12, 14
Cycles at 22,100 psi				
89,400	.000	.026	.014	.016
131,900	.015	.074	.036	.045
157,500	.053	.190	.064	.097
166,200	Failure			

the crack and the associated slip lines in more detail. While the general direction of the slip lines is that corresponding to the trace of a plane of high shear stress in the [111] direction, some of the slip lines cannot definitely be ascribed to a crystallographic plane. The faint slip lines in the lower left corner are parallel to the trace of the $(2\bar{3}1)$ plane. The crack seems to follow the slip lines closely with the exception of steps from one line to another.

The specimen was run for 42,500 more cycles at the same stress, after which the main crack had spread as shown in Figs. 9 and 10. The lower end of the crack, which was growing more nearly in the [111] direction, had grown faster and with less disturbance to the surrounding metal.

Figs. 11 to 14, taken at the same two times as the previous set of figures, show another crack starting from a crystallite. Plastic deformation was rather severe along both ends of the crack. Fig. 3 shows the specimen after failure, which occurred after 34,300 more cycles. The plane seen as a bright surface on the left, and edgewise on the right, was the lower end of the principal crack. A visual check indicated that it contained the [111] direction, whereas the crack shown in Figs. 11 to 14 appeared to contain the $[1\bar{1}1]$ direction. A summary of the rate of crack growth is given in Table 4. From this table it appears that cracks grow at an accelerating rate, and that they grow fastest when the metal is least deformed.

Fig. 15 88X

III-17 19,800 psi for 300,000 cycles
21,800 psi for 146,700 cycles
$S_3 = 0.025$ in. $\phi = 114\frac{1}{2}^\circ$

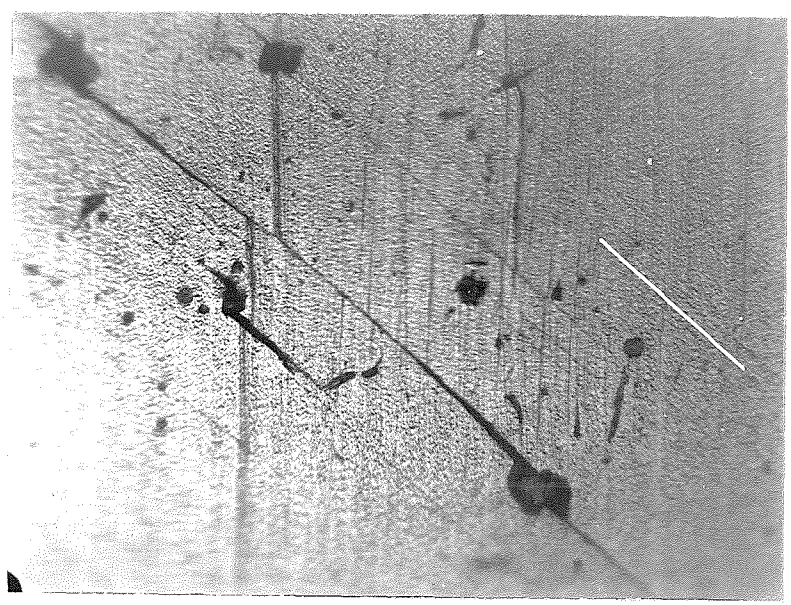

Fig. 16 380X

III-17 19,800 psi for 300,000 cycles
21,800 psi for 146,700 cycles
$S_3 = -.031$ in. $\phi = 11^\circ$
The [111] direction lies on the surface as shown

Specimen III-17

Microscopic observation of this specimen failed to disclose crystallites at any time after it was turned down for the fatigue tests. The polar coordinates of the specimen axis relative to the [100] direction were $\theta = 41.2^\circ$, $\phi = 97.5^\circ$; those of the radius through the index mark were $\theta = 50.3^\circ$, $\phi = -99.2^\circ$. During 300,000 cycles at 19,800 psi the vibration fell from 0.009 in. to 0.003 in. As mentioned in the discussion on the fatigue machine, p. 15, this decay indicates that the elastic limit was reduced below 3000 psi. The specimen was then stopped and examined. The few slip lines present were lighter and more widely spaced, but otherwise similar to the straight set shown in Fig. 5. The load was increased 10% and the machine was found shut off after another 146,700 cycles. The principal cause of failure was a crack which spread half-way through the specimen. The crack was not a plane surface, but did appear to contain the [111] direction.

The region shown in Fig. 15 had been examined at 380X before testing and again after 300,000 cycles and showed no change, so this crack must have developed entirely at the higher stress. It extended only one picture-width in either direction from the region shown. The sides were probably spread apart by the severe deformations in the last few cycles before failure. The crack seems to be composed of two straight lines, one of which corresponds

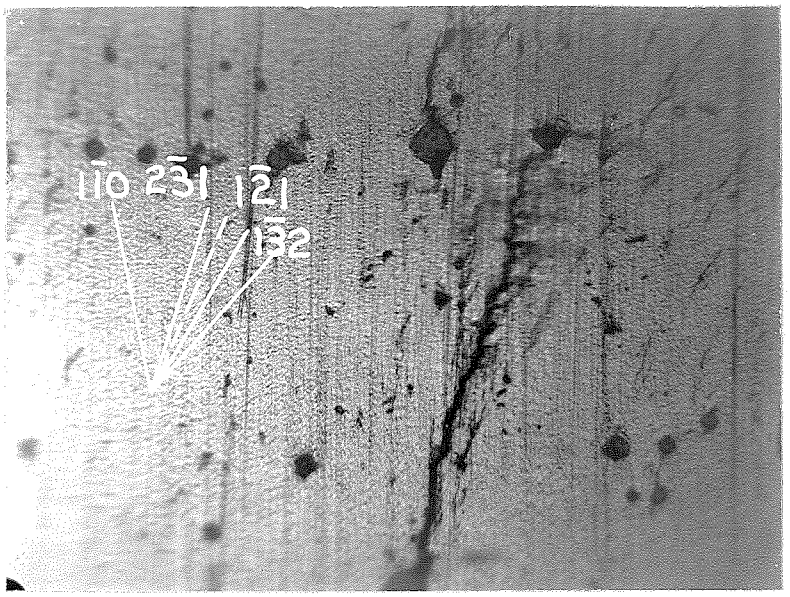

Fig. 17 380X

III-17 19,800 psi for 300,000 cycles
21,800 psi for 146,700 cycles
S_3 = -0.038 in. $\phi = 122\frac{1}{2}^{o}$

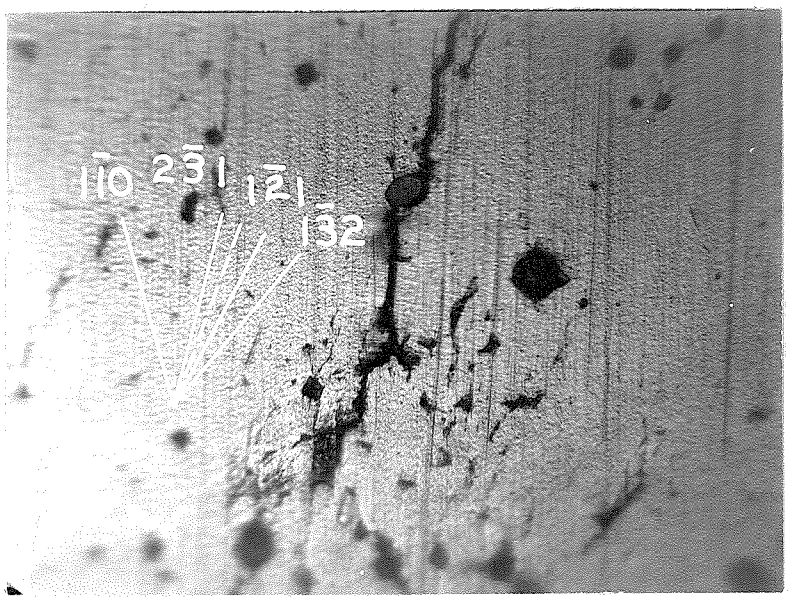

Fig. 18 380X

III-17 19,800 psi for 300,000 cycles
21,800 psi for 146,700 cycles
S_3 = -0.038 in. $\phi = 119\frac{1}{2}^{o}$

to the $(2\bar{3}1)$ trace and the other to the trace of the plane of maximum shear stress.

Another crack is shown in Fig. 16. The [111] direction lies within half a degree of the plane of the surface according to the X-ray analysis. While the main crack is curved, its average direction and the directions of the smaller cracks agree with the [111] direction within the one or two degree accuracy of the calculations. A careful study of the hyperbolic region of focus indicates that there was no appreciable vertical displacement across the crack. Since motion of a half micron in the vertical direction will affect the focus at this magnification and since the crack displacement is about ten microns, the slip direction must lie within 3^{0} of the plane of the specimen at this point. Therefore, the direction of the displacement across this crack lies within a few degrees, at most, of the [111] direction. The influence of inclusions in starting the cracks is evident from the fact that the cracks tend to start from the upper and lower ends of the inclusions, where the stress concentration is a maximum.

Figs. 17 and 18 show another crack starting from an inclusion at a different angular position in the specimen. In this case the [111] direction made an angle of around 40^{o} with the specimen surface. A careful examination of the field of focus at the top of Fig. 18 shows a discontinuity in the surface across the crack. The traces of

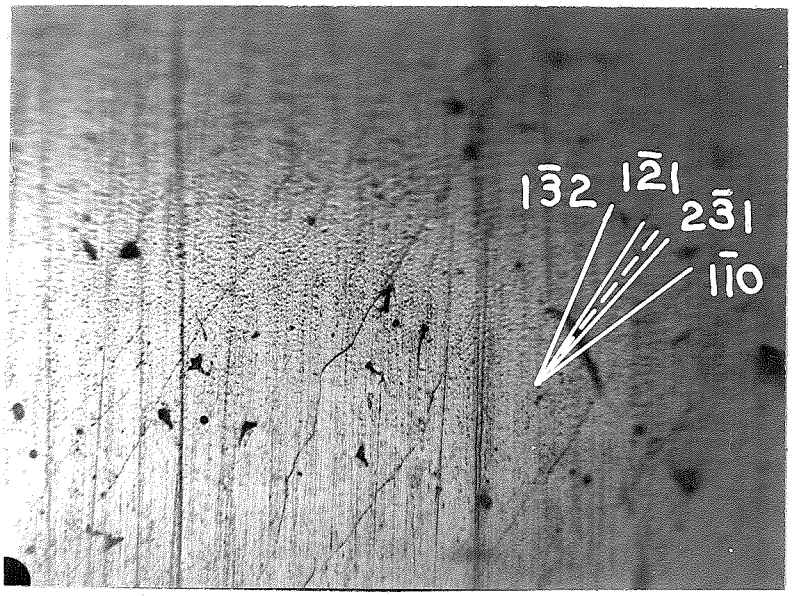

Fig. 19 380X

III-17 19,800 psi for 300,000 cycles
21,800 psi for 146,700 cycles
S_3 = 0.262 in. ϕ = 242°
Local stress 83% of maximum

TABLE 5

SINGLE CRYSTAL FATIGUE TEST RESULTS

SPECIMEN NO.	IV-16	VIII-16	V-4	V-6	V-22	V-16	III-17
SURFACE FINISH	ZIG-ZAG POLISH	ETCHED	ETCHED	POLISHED	ETCHED	ETCHED	ETCHED
FIRST STRESS, PSI TENSILE	31,500	20,000	25,000	21,700	20,000	20,000	19,800
INITIAL VIBRATION, IN. PEAK TO PEAK	>.015	.0035	.0025	.0005	.0018	.0008	.009
VIBRATION DECAY	YES	NO	YES	NO	NOT BEFORE 36,000 CYCLES	NO	YES
CYCLES	11,200	318,000	32,500	31,700	295,000	381,000	300,000
SECOND STRESS, PSI TENSILE	-	22,000	-	-	-	22,100	21,700
CYCLES	-	149,000	-	-	-	166,200	146,700
CAUSE OF FAILURE	-	LARGE CRYSTALLITE	SCARF JOINT	CRYSTALLITES	2 CRACKS, 1 FROM CRYSTALLITE	2 CRYSTALLITES	INCLUSIOUS
$\frac{\tau_{\langle 111 \rangle\ MAX}^{*}}{\tau_{MAX}}$	-	.993	-	.940	-	.998	.988

$$^{*}\frac{\tau_{\langle 111 \rangle\ MAX}}{\tau_{MAX}} = \frac{\text{MAX SHEAR STRESS ON PLANE CONTAINING } \langle 111 \rangle \text{ DIRECTION}}{\text{MAX SHEAR STRESS}}$$

different crystallographic planes are shown, but do not seem to have much to do with the crack direction. There is less disturbance of the metal around the ends of this crack than around the ends of the cracks in Specimen V-16.

Fig. 19 shows a region of lower stress where the beginnings of slip lines can be seen at an early stage. Most of the lines can be resolved into segments parallel with one or another of the traces shown, but some segments lie in between.

Other Specimens

Other single crystals tested were even more imperfect than those discussed above. These were not analyzed in detail, but the failures were similar in general appearance to one or another of those described above. A summary of all tests is given in Table 5. The last row of this table gives the ratio of the maximum resolved shear stress on a plane containing a ⟨111⟩ direction to the maximum shear stress in the specimen. Very likely strength of single crystals of iron will sometime be correlated on the basis of this resolved shear stress. Since the crystals tested were not uniform enough to warrant such a correlation, the strength is given in terms of tensile stress so that it may be more readily compared to the polycrystalline test results.

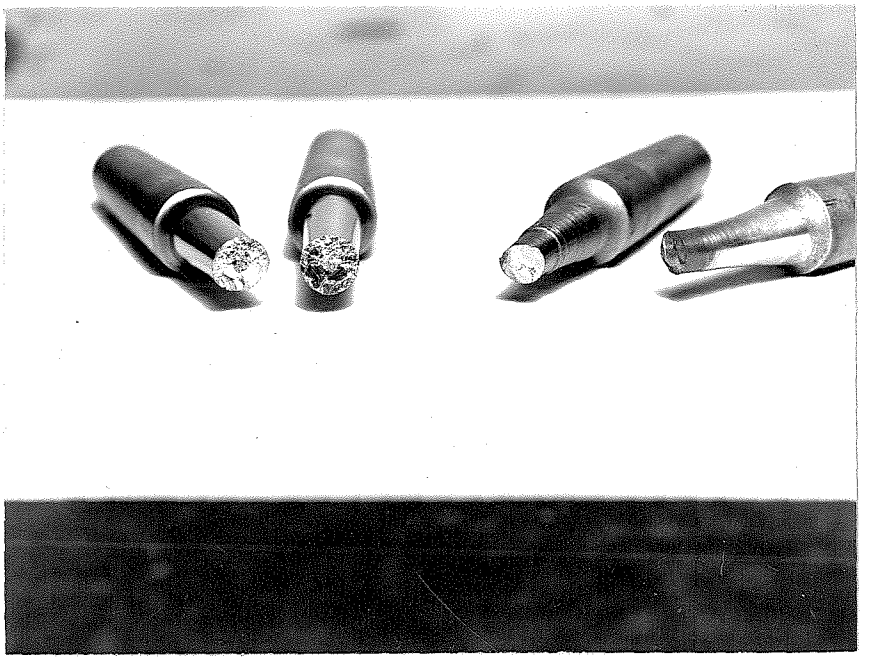

Fig. 20 1X

Cleavage Fractures

IV-18
Intercrystalline fracture above

Cleavage on cube face below

IV-4
Cleavage on cube face

Cleavage Failures

Specimen IV-18

This specimen, which consisted of two large crystals joined near the center, was run in order to investigate the strength of the weak grain boundaries under repeated stress. After withstanding 50,000 cycles at 12,000 psi, and 55,000 cycles at 14,500 psi, it broke after a further 16,000 cycles at 17,280 psi. As shown in Fig. 20, the fracture occurred principally along the grain boundary, which is a dimpled surface. In part, however, it traversed a projection of one of the grains with a plane fracture. The coordinates of this plane were measured by reflecting light from it. The cleavage plane was found to be three degrees from the calculated (100) plane. While a total error of two degrees was all that was expected, the surface probably was that of a cube face.

Specimen IV-4

Specimen IV-4, which was broken in machining, is also shown in Fig. 20. In this case the specimen was too badly curved to use the light reflection method so the coordinates were estimated by eye. The estimate was five degrees from the coordinates of the cube face as determined by X-ray analysis. Certainly, if these planes represent crystallo-

graphic planes of reasonably low indices, they are {100} planes. This is the plane in which cleavage has previously been reported by Barrett, Ansel, and Mehl (6), although not at room temperature.

Discussion of the Single Crystal Fatigue Test Results

The character of the slip surfaces in iron cannot be finally determined by this new set of observations. Gough (4) has shown a picture of quite straight intersecting pairs of slip lines, stating that these develop into wavy lines later. The present series of pictures shows that such is not always the case. These pictures do however, agree with the hypothesis that slip occurs in the ⟨111⟩ direction. Whether the wavy surfaces are really made up of sets of submicroscopic planes of definite crystallographic directions is a problem that must be left to the electron microscope. The cause of the wavy surfaces will not be clear until someone can produce both wavy and straight lines at will, as Greenland (18) did with mercury. He found that preliminary bending caused wavy lines to appear when the specimen was loaded in tension. In iron, it may be that impurities affect the slip surfaces.

Some of the fatigue cracks follow slip surfaces, at least in steps. Others distort the metal so badly that details cannot be seen. The general direction of these cracks may not follow slip surfaces. On a macroscopic scale, the

cracks follow surfaces of high shear stress which apparently contain a ⟨111⟩ direction. The surfaces are not always ones of maximum shear stress, as Gough (4) suggested, for the crack in Fig. 16 makes an angle of less than 45° with the specimen axis.

The stress at which single crystals will fail in 300,000 cycles of rotary bending is somewhere between 20,000 and 30,000 psi tensile stress. This is in accord with Gough's finding of 118,000 cycles at 16,200 psi shear stress (3). The fatigue strength of single crystals of iron is thus of the same order as that of polycrystalline iron, which is about 24,000 psi tensile stress for the same life. This agreement is probably a coincidence, for one would expect the fatigue strength to be lower due to a reduced yield point, and higher due to the absence of intergranular stress concentration.

TABLE 6

ROTARY BENDING TESTS ON POLYCRYSTALLINE INGOT IRON; KILOCYCLES TO FAILURE

GROUP No.	CONDITIONS OF TEST (27,000 PSI AND 794 RPM UNLESS OTHERWISE NOTED)	BAR II		BAR IV		BAR V		BAR VI		BAR VII		BAR VIII		BAR IX	
		No.	Kc.	No.	Kc.	No.	Kc.	No.	Kc.	No.	Kc.	No.	Kc.	No.	Kc.
1	27,000 PSI 3,800 RPM					1 9 18	334 1322 582								
2	30,000 PSI 3,800 RPM	10	108			13 19	124 192								
3	STANDARD CONDITIONS	14 16	3065 2065	9[A] 17[A] 21[A] 7[A,B] 15[A,B] 23[A,B] 3[A,C] 13[A,C] 25[A,C]	139 127 144 108 116 113 94 109 99	5 11 17	250 425 385	5 9 21 12[A]	364 877 389 109	6 14 16	259 124 366	1 9 15	338 360 288	1 7 15	233 318 270
4	30,000 PSI 794 RPM					3	100	3 13 19	383 126 111	10	107				
5	COAX TO 29,300 PSI													3	674
6	1640 F STRESS RELIEF AFTER MACHINING (24,000 PSI)											5 11 13	88 113 292		
7	ANNEAL, RUN											17	122		
8	ANNEAL, POLISH, RUN	8 12 18	81 62 66			15	116	7	114	6 8	111 110				
9	ANNEAL, RUN AND REPEAT AFTER KC DENOTED ( )											3	103 (60)	5	173 (30)
10	ANNEAL, POLISH, RUN AND REPEAT AFTER KC DENOTED ( )							1 11	30[D] (30) 102 (60)			7	180[+] (30)	9[E] 13[F]	120 (7 1/2) 135 (15)

A. ANNEALED AT 1,700 F 1 HR; COOLED AT 100 F/HR
B. MACHINED WITH A MECHANICAL FEED
C. ANNEALED AT 1,700 F 1 HR AND 1,630 F 5 HR; COOLED 100 F/HR
D. NOT RUN TO FAILURE
E. ANNEALED 12 TIMES AND THEN RUN TO FAILURE
F. ANNEALED 2 TIMES AND THEN RUN INTERMITTENTLY TO FAILURE

IV: POLYCRYSTALLINE FATIGUE TESTS

The objects of the polycrystalline fatigue tests were to check the behavior of the polycrystalline ingot iron against the results of previous investigators, and to study the cracks from the earliest stages possible. The tests were made on standard Moore-type fatigue specimens with the rotary bending fatigue machine previously described. No attempt was made to determine the endurance limit or study the cycles to failure at a wide variety of stresses, since this has been done before. The stress at which most of the tests were run, 27,000 psi, was chosen to give a life of the order of hours at the speeds used. Thus there was plenty of time to make macroscopic observations during a test, but the total time to failure was not excessive.

The results of the polycrystalline fatigue tests are shown in Table 6. In view of the scatter present in these data, it is worthwhile to apply statistical methods to decide whether apparent differences in the fatigue life may be due to scatter or whether they were probably caused by the various treatments. It will be assumed that the logarithm of the cycles to failure of a homogeneous group of specimens is normally distributed in order that Student's t-distribution (19) may be applied. While the normality assumption is not strictly correct, the error in the results due to skewness which may be present is not considered important. It is desired to make some statement regarding

the mean of the logarithm of cycles to failure which might be expected if one were able to repeat the experiments an indefinitely large number of times. 98% confidence limits will be given for the means. That is to say, limits within which these means lie will be deduced from the data by statistical methods which are correct 98% of the time they are applied if the underlying assumption for normality is valid.

The results will be described in two sections: introductory tests and crack detection tests.

Introductory Tests

Groups 1 and 2 of Table 6:

The first tests were run at 3800 rpm which was above the critical speed of the fatigue machine. There was so much general vibration of the machine and its support that the remaining polycrystalline tests were run at 794 rpm.

Group 3 of Table 6:

The long life of specimens from Bar II was probably due to polishing them in the fatigue machine without locking the bearings so that the forces inadvertently applied during polishing caused considerable understressing of the specimens.

Bar IV will be discussed later.

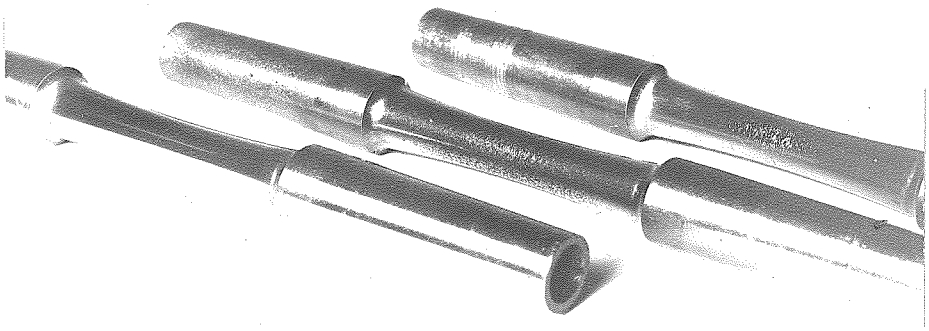

Fig. 21 1X

Surface Conditions at Failure

All specimens were annealed at 1700 F one half hour, furnace cooled with an initial rate of 450 F/hr, and then machined and polished. Further treatment is described below.

IX-7	VIII-17	VIII-5
	Annealed at 1700 F/hr	Stress relieved at 1630 F for 5 hrs
	Cooled at 100 F/hr	Cooled at 100 F/hr
27,000 psi for 318,000 cycles	27,000 psi for 122,000 cycles	27,000 psi for 88,300 cycles

Bar VII was notable for the number of inclusions visible even without the aid of a microscope, but there seemed to be no tendency for the cracks to start from them. Principally as a result of Specimen VII-14, the average life of specimens from Bar VII appears to be lower than that of specimens from the other bars. If the material from Bar VII were the same as the rest, there is only one chance in twenty that lives as short or shorter than these would be obtained. We can therefore say that the tests indicate, but do not prove, that specimens from Bar VII were weaker. For the time being, therefore, specimens from Bar VII were not included in the comparisons.

The mean life of specimens from the remaining bars annealed in the hearth furnace, Bars V, VI, VIII, and IX, is 270,000 to 460,000 cycles. Moore and Kommers ran tests on similar specimens of ingot iron described as "box annealed" (20) or "normalized" (14). Judging from the five tests at a stress nearest 27,000 psi, their material had a life of 630,000 to 4,000,000 cycles, at that stress. As will be seen below, differences in heat treatment could easily account for this difference. Specimen IX-7, shown in Fig. 21, had a failure typical of those in this group. Two to three circumferential cracks caused a failure with little surface deformation. As seen with a microscope, the crack zig-zagged, often following slip lines where those were visible.

Specimens from Bar IV were not annealed in the hearth furnace but in the tube furnace. They were annealed in a hydrogen atmosphere and cooled at a rate of 100 F/hr. Six specimens were annealed at 1700 F for one hour and three were annealed at 1700 F for one hour followed by a further anneal at 1630 F for five hours. Three of the first group were machined with a hand-feed as were the specimens from other bars. The remaining specimens of Bar IV were machined in another shop with a mechanical feed. The effect of the anneal at 1630 F is not clearly determined. There is about one chance in fifteen that lives as short as or shorter than those obtained with the longer anneal would be found if the material were the same. The difference in machining technique is significant, however. The mean lives resulting from the two techniques differ by a factor which lies between 1.02 and 1.43. The scatter and mean life in specimens from Bar IV are definitely different from the remaining bars. The question remains whether this difference is due to the material itself or to slow cooling after the anneal in the tube furnace. At this stage only one specimen from the other bars was still unmachined. That specimen, VI-12, was annealed in the tube furnace, cooled at 100 F/hr, and machined in the hand-feed set-up. The mean life of specimens treated this way is somewhere between 12% and 83% of the life of specimens annealed in the hearth furnace, cooled at 450 F/hr, and machined in the

same shop. Therefore the annealing and not the peculiarity of the material of the specimen from Bar IV is probably the cause of the short life. The scatter in the location of failure in the specimens from Bar IV was the same as that for the other bars. The difference in variation of life between Bar IV and the remaining bars must therefore be due to differences from specimen to specimen rather than different variations within the specimens. The variations in the lives of specimens from Bar IV was more nearly in line with that expected from the variation in the location, so there must be some lack of homogeneity in the specimens from the remaining bars. Since no correlation was noted between the position of specimens in the furnace during the annealing and their lives, the lack of homogeneity is probably due to variations in machining. The specimens from Bar IV which were machined by the same technique were likely more carefully machined, being in a smaller group. It was in order to eliminate machining effects that the single crystals were alternately etched and polished.

Group 4 of Table 6:

The few tests run at 30,000 psi indicate the expected reduction in life at a higher stress.

Group 5 of Table 6:

Specimen IX-3 was run 1,000,000 cycles at stresses

of 20,000, 22,000, 24,200, and 26,600 psi. It finally failed after 674,000 more cycles at 29,300 psi. This result is in accord with Kommers' finding (14) that ingot iron could be strengthened by understressing.

Group 6 of Table 6:

Specimens VIII-5, VIII-11, and VIII-13 were stress relieved at 1630 F for four hours in the tube furnace and cooled at 100 F/hr. They had previously been annealed in the hearth furnace, machined, and polished. The surface of these specimens was quite dimpled as compared to that of the specimens without the stress relief. Fig. 21 shows Specimen VIII-5 after failure. The life of these specimens was markedly shortened by the stress relief.

Group 7 of Table 6:

Specimen VIII-17 was annealed at 1700 F after machining. Its life was shortened and the surface of the specimen was not only dimpled, but also certain of the grains seemed to be oxidized in a number of places, as can be seen from the lower side of the specimen in Fig. 21.

Group 8 of Table 6:

A number of specimens which had been previously machined and polished were annealed in the tube furnace, cooled at the usual rate of 100 F/hr, and then re-polished.

Fig. 22 88X

VIII-3 Annealed at 1700 F 1 hr; cooled at 100 F/hr
27,000 psi for 60,000 cycles
S_3 = -0.05 in. ϕ = -32°

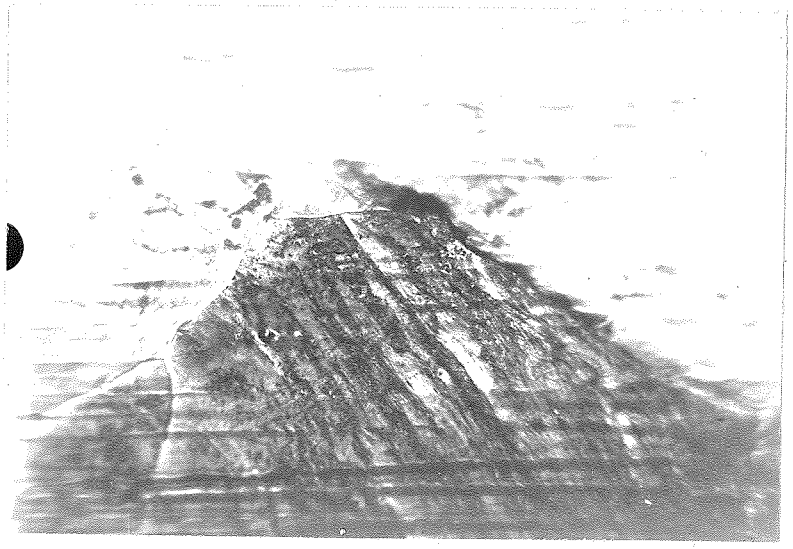

Fig. 23 380X

VIII-3 Annealed at 1700 F 1 hr; cooled at 100 F/hr
27,000 psi for 60,000 cycles
S_3 = 0.18 in. ϕ = -65°

At failure the surface on these specimens was dimpled, but not oxidized, and was similar to that of Specimen VIII-5 shown in Fig. 21. The results fell into two different groups. The specimens from Bars V, VI, and VII had similar lives, and one would expect other specimens from the same material to have average lives of 106,000 to 120,000 cycles. On the other hand, the average life of specimens from Bar II would be between 40,000 and 120,000 cycles with significantly more scatter. The author knows of no reason for the difference, but it was noted that the specimens from Bar II seemed to have a more badly deformed surface than the others.

Crack Detection Tests

Group 9 of Table 6:

In order to learn something about the formation and propagation of cracks, a number of specimens were given an examination at 88X after a fraction of their expected lives. The examination covered about 0.4 in. in the center section of the specimen and required two to four hours to complete, including examination of regions of special interest at 380X and a half dozen photomicrographs.

Specimen VIII-3 was run for 60,000 cycles and then examined with the microscope. Fig. 22 shows an area containing a crack at 88X. The crack runs diagonally between

two grains and then up into a single grain. Fig. 23 is a photomicrograph at 380X of another point showing in more detail the oxidation taking place on the surface. The author feels that this is really oxidation and not massed slip lines reported by others (8), (9), (10) because of the brown and blue colors observed. So many cracks were seen in this specimen that failure was believed imminent. After another 30,000 cycles, however, the cracks had grown only a limited amount and the specimen was reannealed. It did fail after the next 12,800 cycles.

IX-5 was then run for 30,000 cycles. The surface was again oxidized and distorted, so that although no cracks were seen, some may have been present. It was thought that if no cracks were present, annealing should return the specimen to its original state, and further running and annealing should not cause failure. If, on the other hand, cracks were present, the annealed specimen would still be in a damaged condition and would fail eventually. In other words, it was hoped that a cycle of alternate running and annealing would distinguish between cracks and other surface markings. Specimen IX-5 failed after a total of 173,000 cycles, with reannealing every 30,000 cycles. The surface became so badly distorted that microscopic examination was impossible. It was therefore decided to repolish after annealing in order to avoid oxidation and have a better chance of finding out when cracks occur.

Fig. 24 88X

VI-11 27,000 psi for 60,000 cycles
S_3 = 0.08 in. ϕ = 154°

Fig. 25 88X

VI-11 27,000 psi for 102,400 cycles with reanneal and repolish
0.0006 in. removed from surface
S_3 0.08 in. ϕ = 154°

Fig. 26 380X

VI-1 27,000 psi for 30,000 cycles
S_3 = -0.02 in. ϕ = $-7\frac{1}{2}^{o}$

Fig. 27 380X

VI-1 27,000 psi for 30,000 cycles
Etched 20 sec. in 10% HNO_3 in methanol
S_3 = -0.02 in. ϕ = $-7\frac{1}{2}^{o}$

Group 10 of Table 6:

Specimen VI-11 was annealed, repolished, and re-run for 60,000 cycles. Fig. 24, taken at the end of this time, shows what appear to be two cracks in the surface. The diagonal markings on the surface in the lower left corner were due to accidentally striking the specimen during examination. The specimen was then annealed, repolished, and run to failure, which occurred after a further 42,400 cycles. The same area is shown in Fig. 25. The cracks had not been visible after repolishing, but it is evident that the left hand crack had only been covered over. Since only 0.0006 in. was removed from the surface in polishing (less than 1/16 in. at the magnification used), the right hand crack, if such it was, must have been quite shallow.

Specimen VI-1 was run only 30,000 cycles after the first anneal and repolish. Several cracks were found, two of which are shown in Fig. 26. Fig. 27 shows the same region after etching and indicates that the cracks were certainly associated with grain boundaries, although the left hand crack has turned off into a crystal. In order to get some idea of the amount of cold work done on the specimen by the fatigue test, it was annealed first at 1100 F and then at 1300 F, after which a few new grains were seen. 1300 F is the temperature at which iron

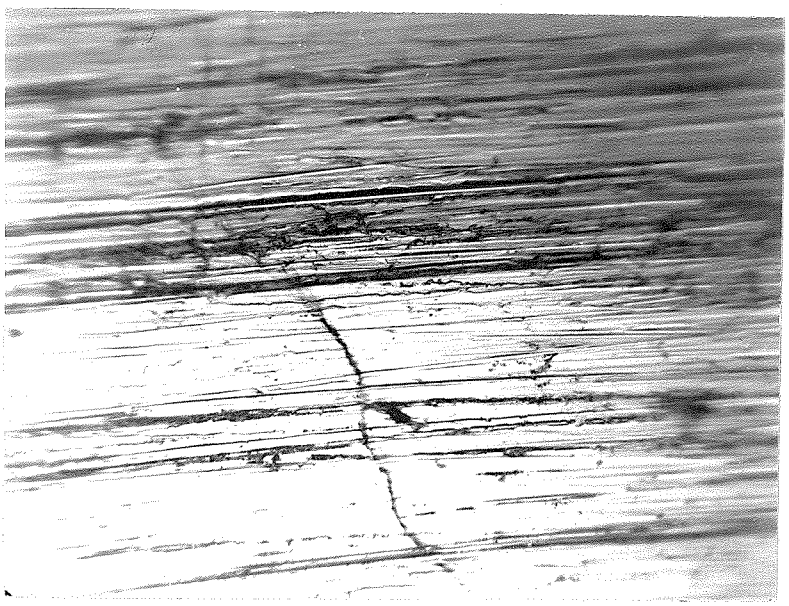

Fig. 28 380X

IX-13 27,000 psi for 30,000 cycles
S_3 = 0.11 in. ϕ = 112°

Fig. 29 380X

IX-13 27,000 psi for 45,000 cycles
S_3 = -0.01 in. ϕ = 58°

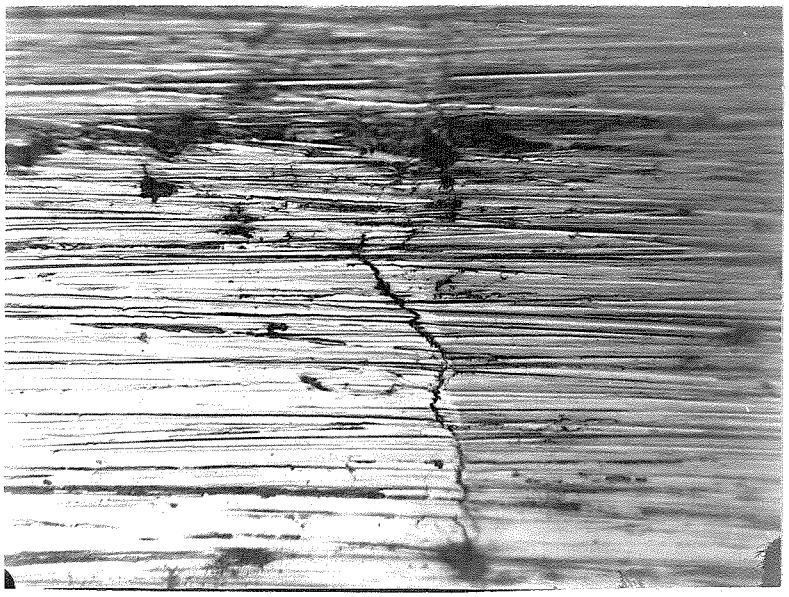

Fig. 30 380X

IX-13 27,000 psi for 60,000 cycles
S_3 = -0.01 in. ϕ = 59°

Fig. 31 88X

IX-13 27,000 psi for 60,000 cycles
Same region as Fig. 29

Fig. 32 88X

IX-13 27,000 psi for 75,000 cycles
Same region as Fig. 29

Fig. 33 88X

IX-13 27,000 psi for 90,000 cycles
Same region as Fig. 29

Fig. 34 88X

IX-13 27,000 psi for 105,000 cycles
Same region as Fig. 29

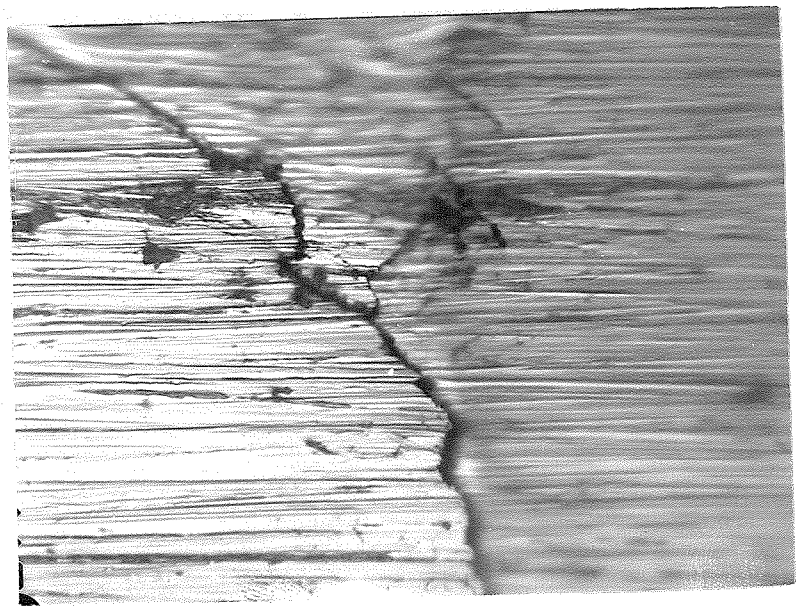

Fig. 35 380X

IX-13 27,000 psi for 105,000 cycles
Same region as Fig. 29

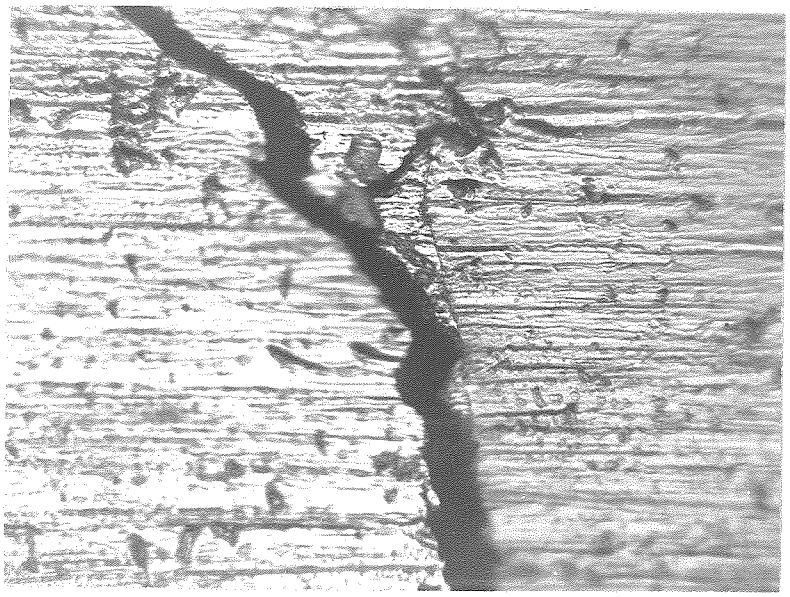

Fig. 36 380X

IX-13 27,000 psi for 120,000 cycles
20 sec. etch in 10% nitric acid
in methanol
Same region as Fig. 29

Fig. 37 88X

IX-13 27,000 psi for 120,000 cycles
20 sec. etch in 10% nitric acid in methanol
Same region as Fig. 29

Fig. 38 88X

IX-13 27,000 psi for 12o,000 cycles
20 sec. etch in 10% nitric acid in methanol
Different region from Fig. 29

deformed 2% by cold rolling will recrystallize, according to Kenyon (21). The specimen was not run to failure. Specimen VIII-7 was also reannealed every 30,000 cycles. Cracks were observed after the first running, but the specimen did not fail until after 180,000 cycles.

Specimen IX-13 was then run for 15,000 cycles and nothing which could be definitely called a crack was visible. After 30,000 cycles a few questionable lines appeared such as that shown in Fig. 28. These disappeared on annealing, repolishing, and rerunning for another 15,000 cycles. The crack shown in Fig. 29 was noticed this time, however, and it was decided to run the specimen to failure and watch the crack grow rather than to continue with the annealing process. The resulting series is shown in Figs. 30 to 35. The out-of-focus blobs along the edge of the crack in Fig. 35 were apparently rust "flowers", for they came into focus above the rest of the specimen and were orange brown in color. They are probably due to the same thing as the frettage corrosion which is observed in press fits under alternating stresses. They were observed in cracks in other specimens as well. After a total of 135,000 cycles, the fatigue machine was beginning to run rough, indicating that failure was imminent, so the test was not continued. Figs. 36 and 37 show the crack, which was the major one of the specimen, after etching for 40 seconds in 10% nitric acid in methanol. The crack

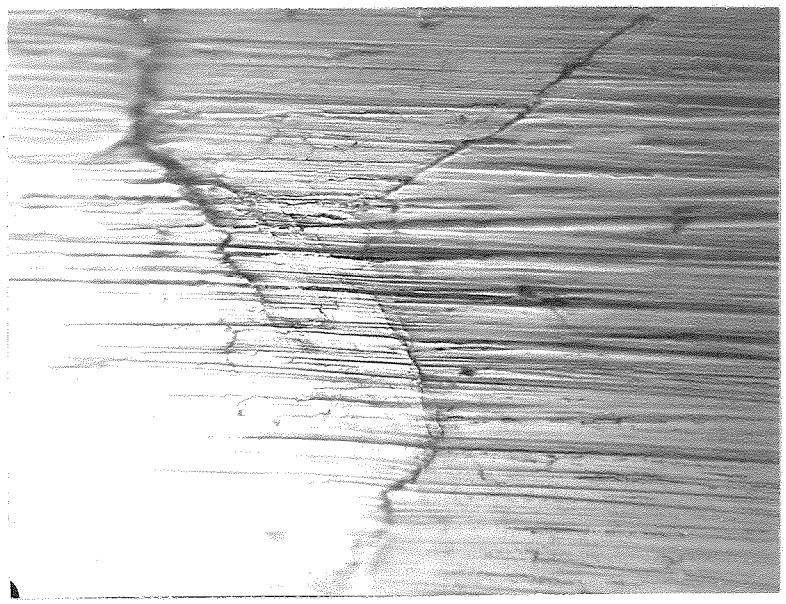

Fig. 39 380X

IX-9 27,000 psi for 75,000 cycles
S_3 = 0.14 in. ϕ = 58°

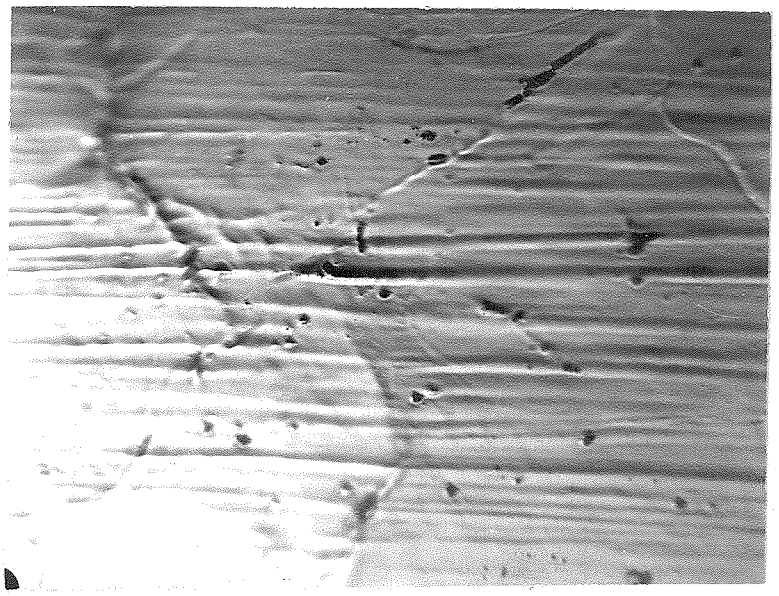

Fig. 40 380X

IX-9 27,000 psi for 75,000 cycles
Same region as Fig. 39 after 1 hr at 1700 F

evidently started near the boundaries of a very large grain. Fig. 38 shows a crack in another part of the specimen where the grain size was more nearly normal. It should be noticed that the crack usually cuts across the grains, but occasionally follows the grain boundaries as described by Lucas (11) and Ewing and Humphrey (8).

Specimen IX-9 was run for periods of 7,500 cycles at a time. At first only a few slight dimples occurred in the surface and nothing that could possibly be called a crack was seen. After more and more repetitions of the anneal-polish-run process, the number and depth of the dimples increased. Finally after a total of 90,000 cycles definite cracks were seen such as those shown in Fig. 39. Fig. 40 shows the same region after annealing. The cracks seem to have healed in many places although one still may be open in the upper right corner. Since almost the entire picture consists of a single grain, the grain size must have been larger than 25 grains/mm^2. After Fig. 40 was taken, the specimen was repolished and run to failure, which required another 30,500 cycles. Judging from the size of the dimples on the surface, the grain size appeared to be of the order of 4 grains/mm^2 or ASTM # -1.

Discussion of the Polycrystalline Fatigue Test Results

This lot of ingot iron appears to behave normally when annealed in the hearth furnace, cooled at 450F/hr,

machined, polished, and run. Since the chemical analysis and tensile test results are also normal, the conclusions drawn should be valid for ingot iron in general.

The rate of cooling of ingot iron has a marked effect upon its life at 27,000 psi. Apparently cooling at 450 F/hr is rapid enough so that any cementite is precipitated in a fine enough manner to harden the material, whereas a cooling rate of 100 F/hr is slow enough to allow the cementite to accumulate in large particles which, though submicroscopic, do not seriously hinder slip. Therefore it is insufficient to describe ingot iron as "annealed"; the cooling rate must also be given.

The surface preparations studied do not have a great effect on the fatigue life. Provided that they were slowly cooled, specimens annealed, machined, and polished; those machined, polished, and annealed; and those machined, polished, annealed, and repolished, all exhibited lives between 90,000 and 125,000 cycles at 27,000 psi with the exception of specimens from Bar II. But the surface preparation does affect the character of the surface during the fatigue test. Specimens machined and polished after the anneal showed a few surface dimples with no discoloration. Specimens annealed just before running showed marked surface deformation and oxidation of individual grains.

Cracks were observed after 30,000 cycles in specimens

whose life very probably would have been no less than 106,000 cycles. The cracks started near grain boundaries, which is in contradiction to Gough's results for large crystals of aluminum (4). In these tests the apparent cause of cracking was the severe deformation at the grain boundaries. As the cracks grew, they usually traversed grains in a zig-zag manner. The average direction of the cracks was normal to the specimen axis. The relation of single to polycrystalline crack direction will be discussed further in chapter V.

The alternate running and annealing cycle is not satisfactory for developing submicroscopic cracks. Grain growth occurs during the process, lowering the normally expected life. Furthermore, the annealing may heal cracks of microscopic size. This healing may account for the fact that if a specimen with an expected life of 110,000 cycles is annealed every 30,000 cycles, its total life will be longer than normal, even though it was cracked after the first 30,000 cycles. Apparently when the anneal is carried out after half the expected life, the cracks are so large that the annealing has little effect.

V: THE DIRECTION OF CRACKS IN POLYCRYSTALLINE SPECIMENS

Cracks in single crystal specimens tested in rotary bending progress on surfaces of high shear stress, that is, diagonally across the specimen. On the other hand, the general direction of cracks in polycrystalline specimens is that of a plane of maximum tension or one perpendicular to the axis of the specimen. Microscopic examination shows, however, that the cracks in polycrystalline specimens are not straight, but tend to zig-zag from one crystal to another. This seems to indicate that cracks in both the single crystal specimens and in the individual crystals of the polycrystalline specimens progress on surfaces of high shear stress, and that the average direction of the cracks in the polycrystalline specimens is due to the random orientation of planes of maximum shear stress containing a $\langle 111 \rangle$ direction, in the different crystals. This hypothesis will now be checked in detail.

To simplify the problem, assume that cracks progress only on planes of maximum shear stress. The intersections of these planes with the surface of the specimen will be lines making angles of 45° to 135° to the specimen axis. Assume that after a crack has traversed one grain, it must progress on a surface of maximum shear stress in the neighboring crystals. Although there may be a tendency for cracks to continue on the same surface, the requirement that they progress on surfaces of high shear stress

containing a ⟨111⟩ direction is likely to cause a change of surface. If the crystal orientations are random, the net effect may be considered a random choice of a plane of maximum shear stress in the neighboring crystal. The easiest way to check this hypothesis is to use it to predict the directions that the cracks take on the surface of the specimen and compare the predicted value with that found experimentally.

In accordance with Fig. 41, let S_3 be the specimen

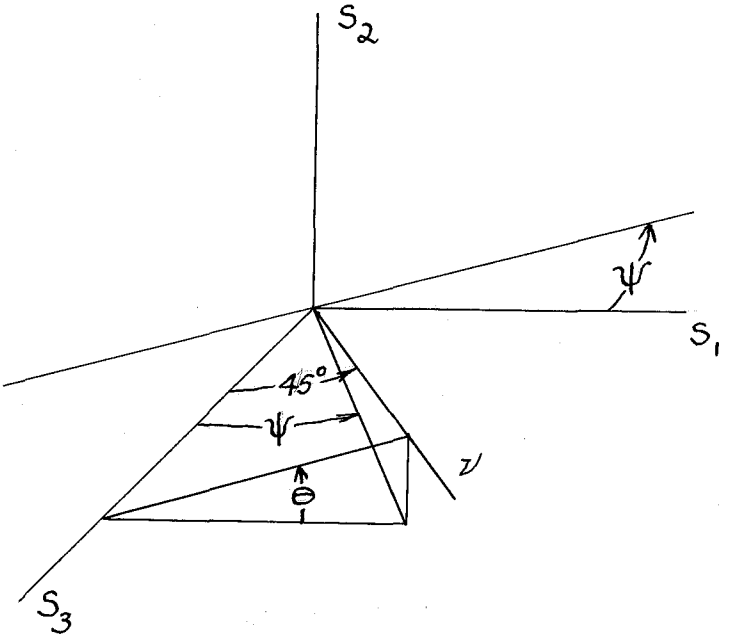

Fig. 41

axis and S_2 the normal to the specimen surface. Let ν be the normal to the plane of maximum shear stress which makes an angle of 45° with S_3. Let ψ be the angle at

which the plane of maximum shear stress intersects the surface. ψ may vary from $+45^{\circ}$ to -45° as ν moves around S_3 in a cone. The relation between ψ and θ is given by

$$\tan\psi = \cos\theta. \tag{1}$$

If all values for θ are equally likely, then the probability that θ will lie between θ and $\theta + d\theta$ is given by

$$p(\theta)\,d\theta = \frac{d\theta}{2\pi} \qquad \text{for} \qquad 0 \le \theta \le 2\pi. \tag{2}$$

Since

$$d\theta = \frac{d\psi}{\cos^2\psi\sqrt{1-\tan^2\psi}}\ , \tag{3}$$

and since the same values for ψ can arise from both positive and negative values of θ, the corresponding probability distribution of ψ is given by

$$p(\psi)\,d\psi = \frac{2\,d\psi}{2\pi\cos^2\psi\sqrt{1-\tan^2\psi}} \qquad \text{for} \quad -\frac{\pi}{4} < \psi < \frac{\pi}{4}. \tag{4}$$

For a crack of unit length the deviation in the S_3 direction is

$$w = \sin\psi \tag{5}$$

Therefore

$$d\psi = \frac{dw}{\sqrt{1-w^2}} , \tag{6}$$

and the distribution function of w is

$$p(w)\,dw = \frac{dw}{\pi(1-w^2)\sqrt{1-2w^2}} \qquad \text{for} \quad -\frac{1}{\sqrt{2}} < w < \frac{1}{\sqrt{2}} . \tag{7}$$

This distribution has zero mean and a variance

$$\sigma_w^2 = \int_{-\frac{1}{\sqrt{2}}}^{\frac{1}{\sqrt{2}}} \frac{w^2\,dw}{\pi(1-w^2)\sqrt{1-2w^2}} . \tag{8}$$

In order to evaluate the integral, change the variable back to ψ :

$$\sigma_w^2 = \int_{-\frac{\pi}{4}}^{\frac{\pi}{4}} \frac{\sin^2\psi\,d\psi}{\pi\cos\psi\sqrt{1-2\sin^2\psi}} . \tag{9}$$

The presence of the trigonometric functions suggests the substitution $z = e^{i\psi}$, whence

$$\frac{\sin^2\psi\,d\psi}{\pi\cos\psi\sqrt{1-2\sin^2\psi}} = \frac{\sqrt{2}\left(z - \frac{z^3}{2} - \frac{1}{2z}\right)dz}{(z^2+1)\sqrt{z^4+1}} . \tag{10}$$

The differential dz is taken as a segment of the unit circle in a counterclockwise direction for $d\psi > 0$. On

the contour shown, Fig. 42, the arguments of these

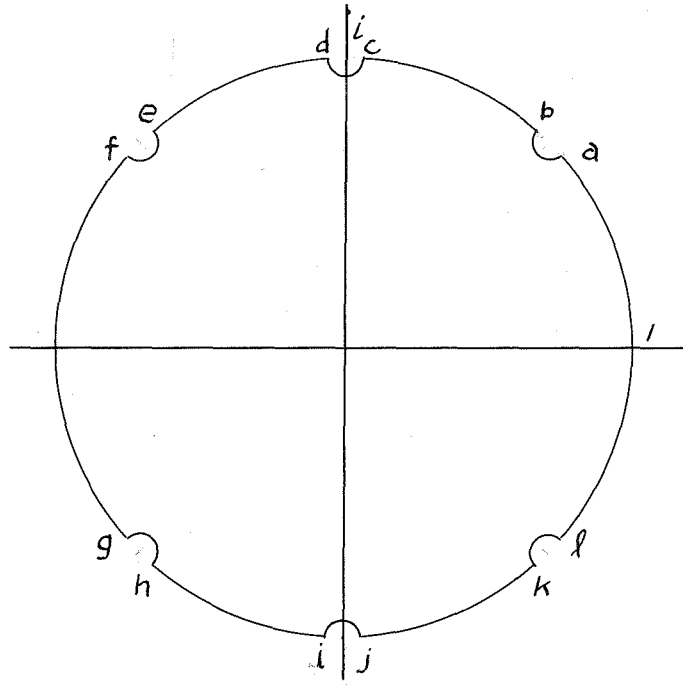

Fig. 42

differentials decrease by $\frac{\pi}{2}$ at $z = \pm\frac{1}{\sqrt{2}} \pm \frac{i}{\sqrt{2}}$ and by π at $z = \pm i$. Therefore the integral from $\psi = -\frac{\pi}{4}$ to $\frac{\pi}{4}$ equals that from $\psi = \frac{3\pi}{4}$ to $\frac{5\pi}{4}$, and the integral will be imaginary elsewhere on the unit circle. The integrals along the indentations at $z = \pm\frac{1}{\sqrt{2}} \pm \frac{i}{\sqrt{2}}$ become vanishingly small as the radii of the indentations approach zero. The integrals along the indentations at $z = \pm i$ are given by

$$\lim \int_i^j = \lim \int_c^d = -\frac{1}{2}\left(2\pi i \operatorname*{Res}_{z=i} \frac{\sqrt{2}\left(z - \frac{z^3}{2} - \frac{1}{2z}\right)}{\pi i (z^2+1)\sqrt{z^4+1}}\right). \qquad (11)$$

Their total contribution to the contour integral is -2.

Now applying the residue theorem to the entire contour, and considering only the real parts

$$\mathrm{RI}\oint = \lim 2\int_{\ell}^{a} - 2 = \mathrm{RI}\; 2\pi i \operatorname*{Res}_{z=0} \frac{\sqrt{2}\left(z - \frac{z^3}{2} - \frac{1}{2z}\right)}{\pi i (z^2+1)\sqrt{z^4+1}} . \quad (12)$$

Finally,

$$\sigma_w^2 = 1 - \frac{1}{\sqrt{2}} . \quad (13)$$

If the crack traverses n grains on the surface, the total deviation in the S_3 direction will be the sum of the deviations across each grain. This total deviation will have a distribution with mean zero and variance equal to the sum of the individual variances:

$$n\sigma_w^2 = n\left(1 - \frac{1}{\sqrt{2}}\right). \quad (14)$$

For a crack of unit length, the progress of the crack in the S_1 direction is given by

$$u = \cos\psi . \quad (15)$$

Therefore

$$d\psi = \frac{-du}{\sqrt{1-u^2}} , \quad (16)$$

and since the same value of u can arise from two values of ψ, the distribution function of u is

$$p(u)du = \frac{2\,du}{\pi u\sqrt{1-u^2}\sqrt{2u^2-1}} \qquad \text{for } \frac{1}{\sqrt{2}} < u < 1 \qquad (17)$$

The mean of this distribution is

$$m_u = \int_{\frac{1}{\sqrt{2}}}^{1} \frac{2\,du}{\pi\sqrt{1-u^2}\sqrt{2u^2-1}} \,. \qquad (18)$$

In order to evaluate (18), change the variable back to ψ :

$$m_u = \int_{-\frac{\pi}{4}}^{\frac{\pi}{4}} \frac{d\psi}{\pi\sqrt{2\cos^2\psi - 1}} \,. \qquad (19)$$

Now substitute $\psi = \frac{\phi}{2}$:

$$m_u = \int_{0}^{\frac{\pi}{2}} \frac{d\phi}{\pi\sqrt{\cos\phi}} \,. \qquad (20)$$

This integral is evaluated by Dwight (22), 854.1:

$$m_u = \frac{1}{2\sqrt{\pi}} \frac{\Gamma\left(\frac{1}{4}\right)}{\Gamma\left(\frac{3}{4}\right)} = .8346 \,. \qquad (21)$$

The variance of the distribution of u is

$$\sigma_u^2 = \int_{\frac{1}{\sqrt{2}}}^{1} \frac{2u\,du}{\pi\sqrt{1-u^2}\sqrt{2u^2-1}} - m_u^2 \,. \qquad (22)$$

Let $\sqrt{1-u^2} = r$; then $\frac{-u\,du}{\sqrt{1-u^2}} = dr$ and

$$\sigma_u^2 = \int_0^{\frac{1}{\sqrt{2}}} \frac{2\,dr}{\pi\sqrt{1-2r^2}} - m_u^2 \qquad (23)$$

$$= \frac{1}{\sqrt{2}} - \frac{1}{4\pi}\left[\frac{\Gamma(\frac{1}{4})}{\Gamma(\frac{3}{4})}\right]^2 = 0.0106\,. \qquad (24)$$

The total length in the S_1 direction of a crack across n grains will therefore be distributed with mean 0.8346 n, and standard deviation $0.103\sqrt{n}$. For large values of n the deviation may be neglected in comparison to the mean value. Then the number of grains of linear dimension g traversed by a crack which progresses for a distance S_1 around the specimen is given by

$$n = \frac{S_1}{.8346\,g}\,. \qquad (25)$$

For comparison with the theory derived above, the three specimens from each of Bars V, VI, VIII, and IX which were run at 27,000 psi and 794 rpm were examined. The grain size found by counting the grains intercepted per unit length of a straight line was 250 to 300 grains/in.

The deviation from the circumferential direction of the center 90° (0.236 in.) was measured for the major crack of each specimen. The number of grains traversed, from Eq. (25), was 71 to 85. The standard deviation of the deviations of these cracks in the axial direction was 0.0238 in., and the 98% confidence interval for the standard deviation of the population from which this sample was drawn is 0.0166 in. to 0.0469 in. The above theory predicts that the standard deviation would be between 0.0167 in. and 0.0183 in. If anything, the cracks are farther from the circumferential direction than predicted. This might be due to a tendency for cracks to continue on the same surface at grain boundaries. The main point, however, is that the theory adequately explains how a shear failure can cause a crack which, from a macroscopic point of view, appears to be on a surface of high tension stress.

In the past, fatigue failures in iron have been thought of as tension failures. The shear failures obtained in torsion tests have been explained by a loss of the statistical isotropy of the polycrystalline material due to cold work (23). The results of this study suggest that fatigue failures are truly shear failures. The axial and circumferential cracks in torsion tests on polycrystalline iron can be explained by a shear failure on a microscopic scale, coupled with a tendency of cracks not to turn a right angle at grain boundaries. The circumferential

cracks obtained in polycrystalline iron in bending tests can be explained by a statistical theory such as that given above.

VI: CONCLUSION

The foregoing study has given further evidence that slip in single crystals of iron occurs in a ⟨111⟩ direction on surfaces of high shear stress which are often, but not always, crystallographic planes of low indices. On a microscopic scale, fatigue cracks follow the slip surfaces with the exception of small steps from one to another. Visual examination of the cracks after failure also indicates that they are surfaces of high shear stress containing a ⟨111⟩ direction.

Tests of more perfect crystals would be of interest in order to confirm these results and to give more quantitative information on the behavior of single crystals under various conditions of repeated stress. Tests of groups of large crystals, provided that they can be obtained with normal grain boundaries, should be made to confirm the observation that fatigue cracks start at the grain boundaries in polycrystalline iron.

The polycrystalline tests also show that in soft iron there is something observable happening throughout the test. Before the initial period of cold work is complete, cracks are beginning to form at the grain boundaries where the cold work has been most severe. These cracks then progress, slowly at first and rapidly later, for the remaining 3/4 of the life of the specimen. In

each crystal the crack progresses along surfaces of high shear stress as it does in the single crystal case. The average direction of the crack across a number of grains is governed largely by chance.

The presence of fatigue cracks as early as 1/4 of the total life of the specimen is of importance for both technical and scientific reasons. If microscopic studies should show that cracks form as early in more common engineering materials, then even more emphasis should be placed on methods of crack detection as a means of preventing fatigue failures in service. Furthermore, the early formation of cracks decreases the hope of any practical form of preventive maintenance, such as re-heat-treatment, for the process would have to be carried out so early and so often as to be prohibitively expensive. The scientific implication of the early presence of cracks is that any quantitative theory of fatigue will have to consider two different phenomena: the formation of cracks of the size of a grain or less, and the growth of those cracks to failure. Neither of these phenomena can be considered of negligible importance in determining cycles to failure at a given stress.

APPENDIX I: CRYSTAL GROWTH

Description of Equipment

An 18 kw. electric furnace was used to heat a fused silica tube, 1 in. ID, over a heated section 12 in. high. At 1640 F the temperature fell off 5 F 1 in. on either side of the center and 20 F 3 in. away. The furnace was controlled by a Micromax 40,000 series controller with a rate of temperature change control. At first a simple on-and-off control was used which caused a temperature variation of ±5F during the cycle. Later an autotransformer was connected so that the controller switched the furnace between two taps close together. This reduced the temperature fluctuation to ± 1½ F. A ten to one reduction gear in the temperature control drive made a temperature rate of 1 F/hr available. The automatic current adjuster on the Micromax controller was connected so that the Micromax would not forget about the furnace while it was balancing itself. An extra dry cell held the current steady enough so that adjustment twice a day was sufficient. The reproducibility of temperature control was limited mainly by the inaccuracy in resetting the control points. For example, in one series of settings on five different days when the control pointer was set through the reduction gear, temperatures measured by an independent thermocouple varied by only ±1 F.

The controller was connected to a chromel-alumel thermocouple located in the center of the furnace just outside the tube. In addition, an iron-constantan thermocouple was placed inside the tube beside the specimen and its output was measured with a Leeds and Northrup portable precision potentiometer. These two couples were intended to provide a mutual check, but the errors increased at about the same rate so that no check could be obtained without recalibration. The couples indicated about 10 F higher than originally after the first 200 hours at 1630 F, and the error increased at a much slower rate from then on. This drift is a good deal more than that reported by Dahl (24), although it shows the same trend of a rapid drift followed by a slow one. The iron-constantan wire was checked by Leeds and Northrup and a correction of 5 F subtracted from the indicated reading at 1650 F. The chromel-alumel thermocouples were checked by putting them with some iron-constantan couples in a 1 in. diameter by 3 in. iron block in the center of the furnace. A helium atmosphere was used to retard the deterioration of chromel-alumel thermocouples which occurs in reducing atmosphere. Impurities in helium are still enough to affect chromel-alumel thermocouples seriously after a few days. A batch of a half dozen iron-constantan couples measured at the same time agreed to ± 1 F. Furthermore, calibration of the chromel-alumel thermocouples on successive days gave as accurate results. The uncertainty

in the drifting rate of thermocouples, however, means that the temperatures reported can only be considered accurate to within ± 5 F or at most ± 10 F. If extreme accuracy is required, it would probably be good practice to season thermocouples for a few weeks before calibration in the atmosphere in which they are to be used.

Hydrogen was fed through a De-Oxo catalytic hydrogen purifier and a 3 in. diameter by 18 in. high drying tower filled with potassium hydroxide. For work with Bar V, a ¼ lb. phosphorus pentoxide bottle was added. Half the powder was still fluffy after 1000 cu. ft. of hydrogen had passed through. The hydrogen line was passed through a dry-ice bottle before and after the furnace in order to check for the presence of water vapor. None was found if the furnace had been flushed out with two to three cubic feet of hydrogen after sealing and if the joints were tight.

After machining, the specimens were annealed one hour at about 1690 F and then cooled at 100 F/hr in the tube furnace. An Olsen universal hydraulic test machine was used for straining. A 2 in. gauge length magnetic strain recorder was mounted on the shoulder to measure the strain. In order to be consistent, the tests were run at an initial stress rate of 4300 psi/min. until the yield point was reached. The valve setting was left untouched until the load began to rise after the yield point, when

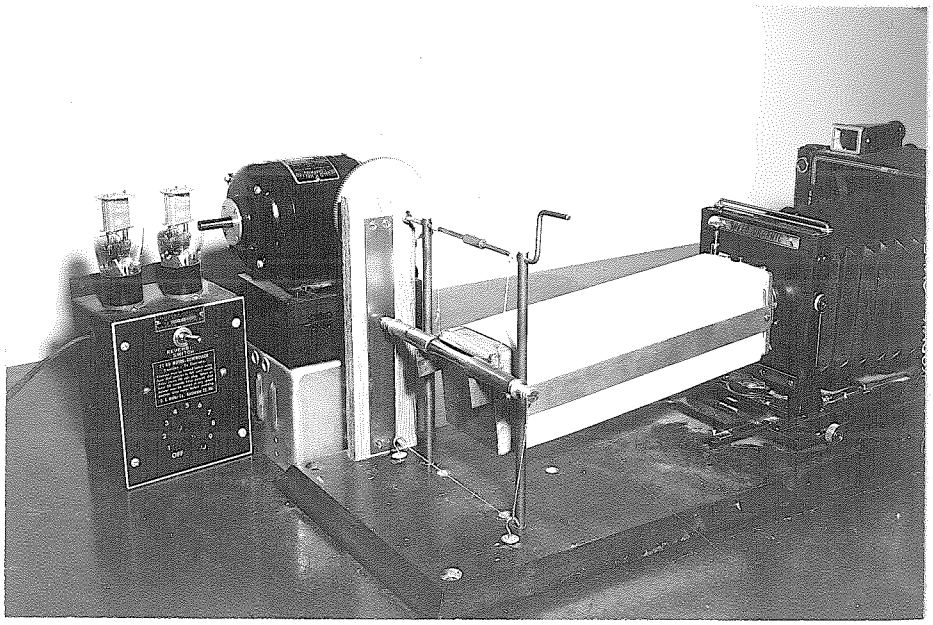

Fig. 43

Apparatus for Circumferential Photographs

the valve was opened so that the stress rate again became 4300 psi/min. Since the range of the stress recorder was only a little over 2%, the test was brought to equilibrium (stress variation of less than 100 psi/min.) and the strain recorder reset to zero. The test was then continued at 4300 psi/min. until just before the desired strain was reached, when conditions were again brought to equilibrium. The load was released and the residual strain recorded both with the magnetic recorder and with a 1 in. micrometer. The magnetic strain gauge readings were multiplied by a factor of 1.185 to account for the fact that the shoulders were not strained as much as the center section. The micrometer readings indicated that this correction was about right for stress of the order of 3%, but gave strains up to 10% too high if the total strain was 4%. The strains reported are the magnetic strains since they are more consistent from one test to another even though there may be a biased error.

The large crystal specimens were photographed with the aid of the apparatus shown in Fig. 43. The camera viewed the specimen through a box with a 0.010 in. slit in the upper left corner. The specimen was mounted on a rack just beyond the slit. As the box was raised by the variable speed motor, a string wound around plugs in the end of the specimen rolled the specimen so that the area just opposite the slit was at the center of rotation and hence stationary.

TABLE 7

CRYSTAL GROWTH: SERIES 1

Spec. No.	Strain	Temp. °F	Hrs.	Result
III-7	.033	1610-45	181	Single crystal shell about polycrystalline core
10	.033	1615-40	100	No growth
11	.033	1625-60	101	One, plus several large ones at one end
12	.033	1640-60	89	No growth
13	.033	1620-55	98	3 longitudinal crystals
14	.033	1630-55	100	No growth
15	.033	1625-50	75	No growth
16	.033	1625-55	87	No growth
17	.033	1635-60	94	Growth started
		1660	56	Further growth of one crystal
18	.033	1625-65	125	No growth
19	.040	1620-55	57	No growth
20	.042	1625-60	125	One large plus several 1/8 in. crystals
23	.033	1615-55	166	1/8 in. crystals
24	.033	1630-50	162	No growth
	.032	1650	23	Two crystals
25	.033	1650	31	No growth
	.032	1650	26	No growth
IV-1	.033	1645-50	71	No growth
2	.028*	1610-40	85	No growth
	.026	1615-45	96	Several large crystals
4	.033	1620-40	56	One, with some untransformed
6	.033	1620-40	83	Several large crystals
11	.028*	1645-55	85	No growth
12	.033*	1620-40	51	1/8 in. crystals
14	.030*	1615-45	100	Several large crystals
16	.025*	1615-35	85	Growth started
		1650	8	Growth complete
18	.033	1625-45	56	Two crystals
20	.026*		39	No growth
22	.033		31	No growth
24	.026*	1615-55	98	No growth
V-2	.038*	1650	64	2 crystals plus flakes and crystallites
4	.030*	1625-50	82	Scarf joint plus flakes
6	.030*	1635	83	Single crystal with crystallites
16	.030*	1645-55	89	" " " "
18	.030*	1640-55	72	2 crystals incompletely grown
20	.030*	1630	33	Several crystals incompletely grown
22	.031*	1645-55	53	Several crystals
VI-4	.030*	1640	77	No growth
	.030	1650-65	28	No growth
14	.030*	1640-50	73	No growth
20	.030	1655	75	No growth

*Annealed 5 hours at 1650°F before further cooling.

TABLE 8

CRYSTAL GROWTH: SERIES 2

Spec. No.	Strain	Temp. °F	Hrs.	Result
II-9	.033	1590-1630	91	No growth
	.032	1635-45	95	1/32 in. grain size
11	.036	1590-1630	91	No growth
	.034	1635-45	93	1/32 in. to 1/16 in. grain size
15	.035	1635-45	93	2 longitudinal crystals
17	.040	1635-45	93	No growth
19	.030	1590-1630	91	No growth
	.029	1635-45	93	1/32 in. to 1/16 in. grain size
VI-6	.039	1635-45	93	Joint in center under crystallites
8	.035	1635-45	93	No growth
10	.032	1590-1630	91	No growth
"	.031	1635-1645	93	1/32 in. grain size
16	.030	1590-1630	91	No growth
	.029	1635-1645	93	1/16 in. to 3/16 in. grain size
18	.035	1590-1630	91	No growth
"	.034	1635-1645	93	1/32 in. to 1/16 in. grain size
VIII-2	.033	1635-45	93	No growth
4	.030	1595-1625	95	No growth
6	.030	1595-1625	95	No growth
8	.033	1635-45	93	No growth
10	.035	1595-1625	95	Joint near one end under crystallites
12	.035	1595-1625	95	Joint in center under crystallites
14	.033	1595-1625	95	Single crystal on one side under skin of crystallites
16	.035	1595-1625	95	Single crystal with crystallites still deep
18	.033	1635-1645	93	Joint in center under crystallites
IX-2	.033	1595-1625	95	No growth
4	.031	1595-1625	95	No growth
8	.035	1595-1625	95	No growth
10	.035	1635-1645	93	No growth
12	.035	1595-1625	95	No growth
14	.035	1595-1625	95	No growth
16	.030	1595-1625	95	No growth

Lighting was furnished by a No. 2 photoflood light 25 in. above and 38 in. behind the lowest position of the specimen. With a film speed of 64 and the camera stopped to f32, a satisfactory exposure was obtained by setting the control at 4 to 10 depending on the surface condition. This resulted in an exposure time of 1/6 to 1/25 sec. Figs. 44 to 48, discussed below, were taken with this apparatus.

Results of Crystal Growth Experiments

Table 7 gives the results of the first series of crystal growth experiments carried out in the tube furnace. The specimen was not held continuously at temperature, but frequently cooled down and examined to find out whether any crystal growth had occurred. Table 8 shows the results of a second series of experiments conducted in a larger hydrogen furnace at the Jet Propulsion Laboratory. In these experiments the examination was made only at the end of a run.

The crystal growth was evidently affected by a number of unknown variables. Some of the irregularities will now be noted.

There seems to be quite a time lag before the initiation of crystal growth. In only a few cases were crystals observed actually in the process of growing. This indicates that once sufficient nucleation time had passed, the

Fig. 44 1X

VI-16
Strain 0.030
1590 F - 1630 F 91 hrs
Strain 0.029
1635 F - 1645 F 93 hrs

Fig. 45 1X

IX-16
Strain 0.030
1595 F - 1625 F 95 hrs
Polish
1635 F - 1645 F 93 hrs

crystals usually grew in less than 24 hours. Of those specimens which were observed in the process of growth, Specimen III-17 grew gradually over a period of 56 hours at 1660 F from the time it was first observed. Specimen IV-16, on the other hand, grew from ¼ in. to a complete specimen in 8 hours at 1650 F. It may be that the number of crystallites present is related to the growth of the crystal, for Specimen III-17 was the only one in which no crystallites were observed under microscopic examination when it was machined for fatigue testing.

After some of the specimens had been run for a long time at temperature with no growth, they were re-strained and reheated. The most successful case of this was Specimen III-24, which contained only two crystals plus crystallites after the final heating. On the other hand, the specimens of Bars VI and IX to which this was done at the Jet Propulsion Laboratory all behaved as if the two strains were simply superimposed, for a number of grains of around 1/16 in. resulted after the second heating. Fig. 44 shows Specimen VI-16, which was one of this group. Since larger grain size is an indication of lower strain, this figure also shows the effect of the constraints due to the shoulders of the specimen and shows that the strain was not uniform around the specimen. Sometimes a single crystal or a number of large crystals were found surrounding the polycrystalline core. Specimen III-7 was thought to be a

Fig. 46 1X

V-22

Extra 5 hr anneal at 1640 F
Strain 0.031
1645 F - 1655 F for 53 hrs

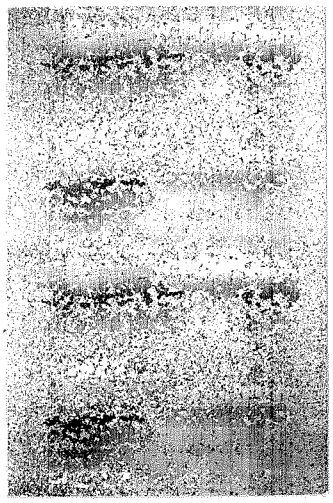

Fig. 47 1X

VI-6

Strain 0.039
1635 F for 93 hrs
Light polish

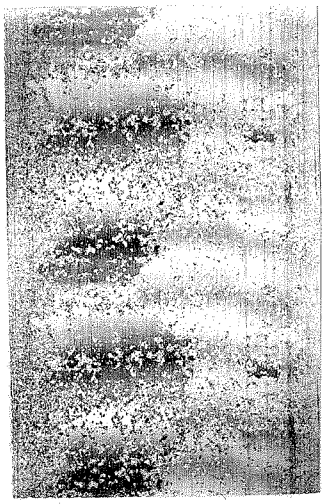

Fig. 48 1X

VI-6

As in Fig. 47, but with
0.003 in. removed

single crystal until it was machined down to 0.22 in. There was only a little of the outside crystal left and the center was made up largely of the original polycrystalline iron. A number of specimens from Bars VIII and IX which failed to grow in the first 95 hours at the Jet Propulsion Laboratory, were, after polishing and etching, reheated for another 93 hours. In all of these a thin layer of large crystals appeared as shown in Fig. 45. Fracture of the specimens revealed that the center was untransformed. Very likely the polishing left enough cold work in the surface to cause recrystallization there. Ziegler (25) noted a similar growth.

When the large crystals grow, they sometimes grow all the way to the surface, as shown in Fig. 46. It is also interesting to note some growth out on the shoulder. Sometimes the surface was covered with a thin section of crystallites, as others have found (13), (25), (26). Figs. 47 and 48 show Specimen VI-6 after a light polish and after removing 0.003 in. from the surface.

As an example of the effect of unknown variables, it should be noted that while Bars VIII and IX had the same grain size within at most a factor of 1.5 on an area basis, and had chemical compositions which could not be distinguished, Bar VIII gave good results with a strain of 0.033 to 0.035, but no growth was observed in Bar IX.

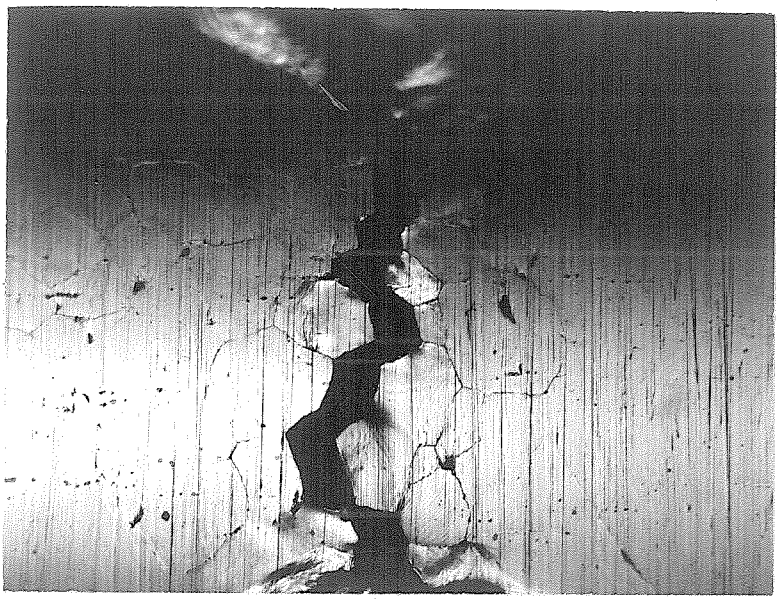

Fig. 49 88X

V-6 21,700 psi for 31,700 cycles

TABLE 9

Summary of Embrittlement Tests

Spec. No.	Prelim. Strain	Temp. °F	Time at Temp. Hrs.	Atmosphere	Cooling Rate °F/hr	Elongation %
III -2	-	-	-	He	100	45
-3	-	1630	40	He	500	10
-4	-	1630	16	H_2	500	40
-5	-	1630	40	H_2	500	45
-6	-	1630	40	H_2	100	40
-14	$3\frac{1}{2}$	1630-60	80	H_2	100	6
-15	$3\frac{1}{2}$	1630-60	80	Partial Vacuum	100	8
-16	$3\frac{1}{2}$	1630-60	80	H_2	100	6
W1	$3\frac{1}{2}$	1630-60	80	H_2	100	10
V -8	-	1630	71	H_2, Sat. 80° F	100	4
-10	-	1630	4	H_2	100	42
-12	-	1630	4	H_2	100	38
-14	-	1630	126	H_2, P_2O_5 dried	100	10

The atmosphere was dried with KOH, except as noted.
All specimens annealed at 1700° before treatment shown.

APPENDIX II: BRITTLENESS IN INGOT IRON

Early in the work it was noticed that some of the specimens which had been around 1640 F for several days broke with a brittle fracture on impact. The intergranular nature of the brittle fractures was observed by piecing ends after a tension test and observing a longitudinal section under the microscope. It is even more clearly shown by Fig. 49, which shows a group of crystallites in a largely single crystal specimen, V-6, after 31,700 cycles at 21,700 psi. This brittleness does affect the fatigue strength, as is shown by the fact that one specimen from Bar II was annealed to make it brittle and failed during polishing in the fatigue machine. The bearings were not locked in this case; even so, the stress could hardly have been over 15,000 psi.

A number of specimens were annealed under different conditions and tensile tests were made on these to learn under what conditions brittleness would occur. These tests are summarized in Table 9. Specimen W1 was machined from a different lot of ingot iron purchased several years earlier.

The Armco Steel Corporation reported in a private communication that this brittleness was due to oxide migration to the grain boundaries. Their chemical analysis showed that there was practically no difference in oxygen

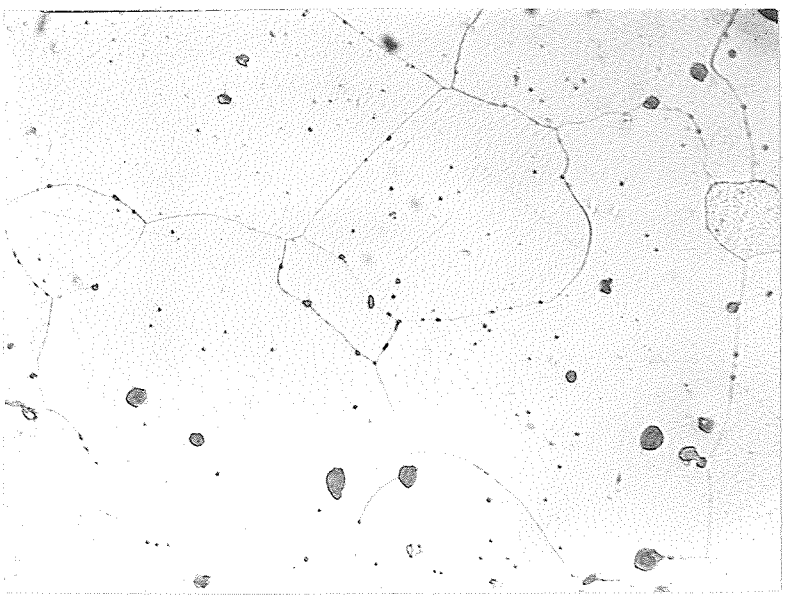

Fig. 50 500X

III-2 1700 F $\frac{1}{2}$ hr
45% elongation

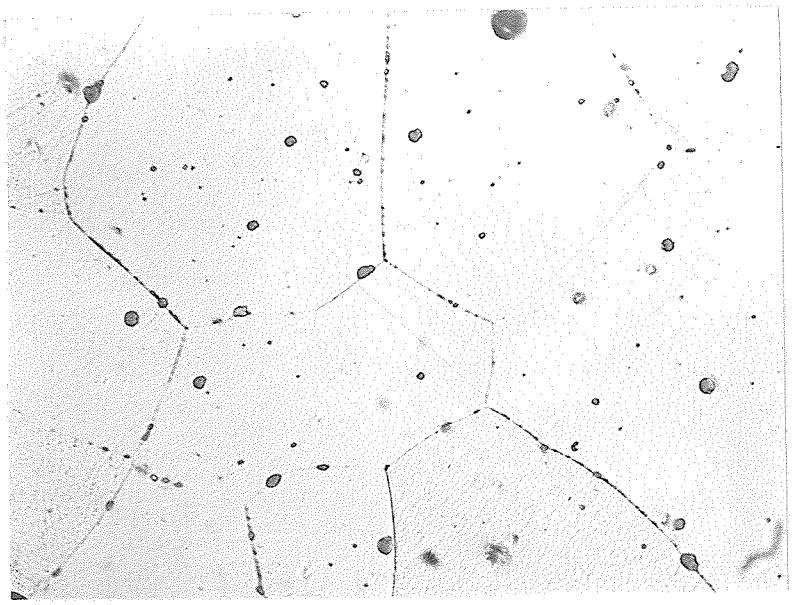

Fig. 51 500X

III-3 1700 F $\frac{1}{2}$ hr, 1630 F 40 hr
10 % elongation

content between the various specimens of Bar V. They did report that the brittleness could be cured by annealing in a hydrogen atmosphere with -50 C dewpoint at 2200 F for 30 hours, but the high temperatures could not be used for the crystal growth work because of the allotropic transformation in iron.

The original microscopic examination of Specimens III-2 and III-3 had failed to reveal any difference between them. A more careful polish, prompted by Armco's results, revealed a marked difference, as shown in Figs. 50 and 51.

The brittleness has previously been reported, both in ingot iron (27) and electrolytic iron (28).

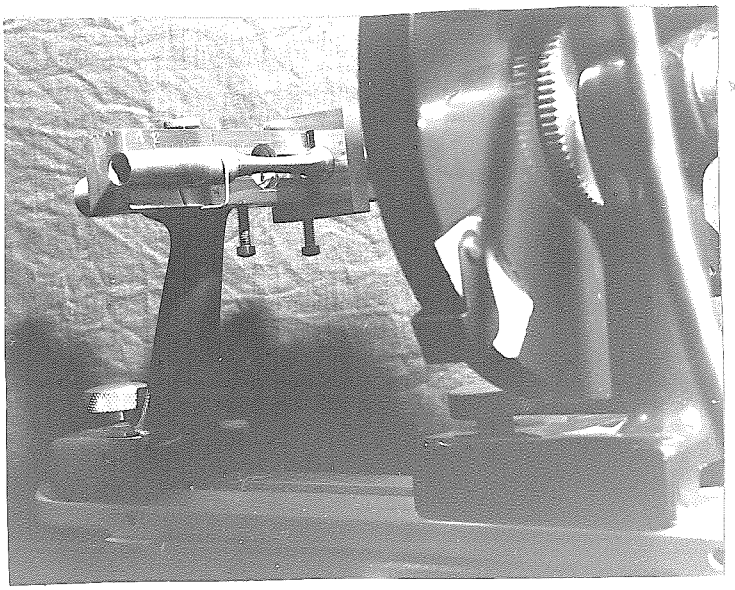

Fig. 52

Specimen Mounted in X-ray Machine

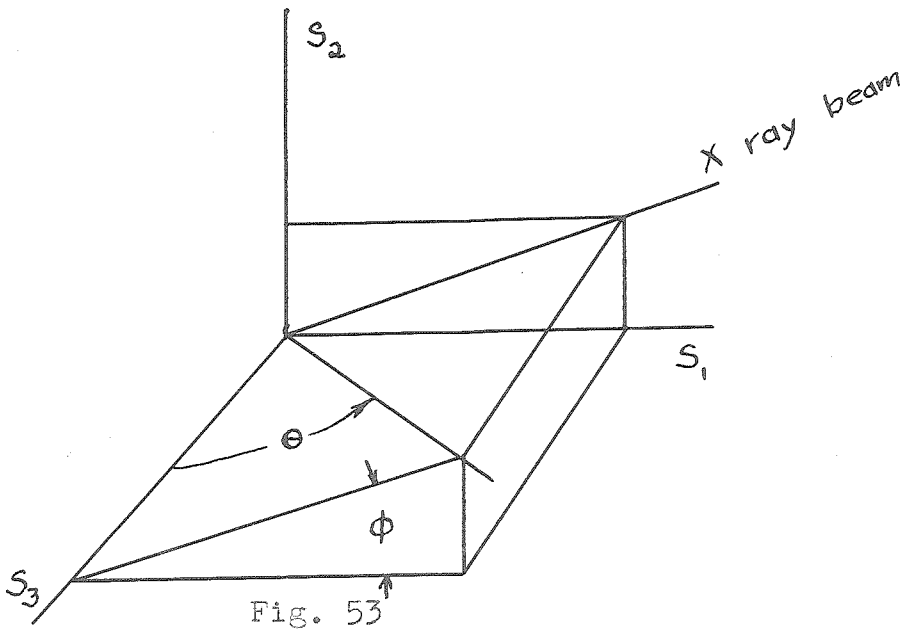

Fig. 53

Specimen coordinates

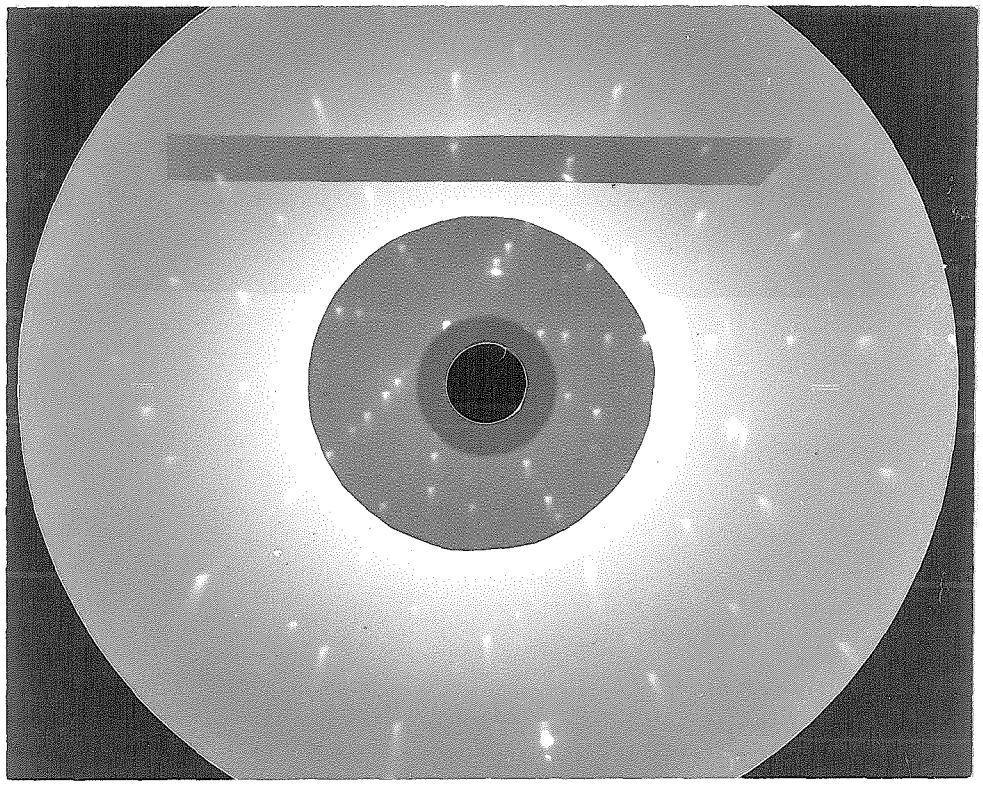

Fig. 54

Back Reflection Laue Diffraction Pattern

Viewed from X-ray Source

Specimen III-17
$\Phi = 0°$
$S_3 = 0$

Molybdenum radiation at 40,000 kv., 15 ma.
.020 in. pinholes
Film-specimen distance 3 cm.
.006 in. aluminum screen over
center part of film

APPENDIX III: THE CRYSTALLOGRAPHIC ANALYSIS OF IRON

Determination of Cubic Axes Relative to Specimen Axes

The orientation of the crystallographic directions relative to the specimen axes was determined from a Laue back-reflection X-ray diffraction pattern. The specimen was clamped in a leveled V block on a Picker X-ray machine. Angular position was determined by the protractor attachment as shown in Fig. 52. The coordinate axes are shown in Fig. 53. The orientation of the film was determined by levelling a 0.006 in. aluminum screen on the face of the film cassette. The resulting pattern for Specimen III-17 is shown in Fig. 54.

The first step in determining crystal orientation from the photograph is to identify the extremely intense spots, often appearing as doublets, which are caused by reflection of the molydenum K_{α_1} or K_{α_2} radiation. The interplanar spacing, d, the wave length of the incident radiation, λ, and the angle between the incident beam and the reflection plane, θ, are related by Bragg's law:

$$\lambda = 2 d \sin \theta \qquad (1)$$

For a cubic crystal the interplanar spacing is given by

$$d = \frac{a}{\sqrt{h^2+k^2+l^2}} \qquad (2)$$

TABLE 10

Diffraction of Molybdenum K_{α_1} and K_{α_2} Radiation by α Iron

Back Reflection Laue Diffraction Pattern

Film-Specimen Distance 3 cm.

Plane	Radius, cm.	
	K	K
444	5.649	5.340
710 , 550 , 543	4.797	4.533
610	4.090	3.857
721 , 633 , 552	3.482	3.272
642	2.943	2.743
730	2.446	2.249
732 , 653	1.474	1.239
800	.890	.501

TABLE 11

ANGULAR COORDINATES OF PLANES IN DIFFERENT ZONES FOR A CUBIC CRYSTAL REFERRED TO PLANE OF MAXIMUM SPACING, D

ENTRIES FOR PLANES WITH $H^2 + K^2 + 1^2 < 60$ AND ZONES WITH H, K, 1 < 4

ZONE 100		ZONE 110		ZONE 111		ZONE 210		ZONE 211		ZONE 221		ZONE 310		ZONE 311		ZONE 320		ZONE 321		ZONE 322		ZONE 331		ZONE 332	
PLANE	ρ	PLANE	ρ	PLANE	ρ	PLANE	ρ	PLANE	ρ	PLANE	ρ	PLANE	ρ	PLANE	ρ	PLANE	ρ	PLANE	ρ	PLANE	ρ	PLANE	ρ	PLANE	ρ
$0\bar{1}7$	-8.1	$\bar{1}17$	-11.4	$54\bar{1}$	-10.9	$\bar{1}27$	-17.7	$\bar{1}3\bar{5}$	-17.0	$54\bar{2}$	-18.4	$\bar{1}37$	-24.3	$\bar{1}3\bar{6}$	-20.2	$3\bar{2}6$	-31.0	$\bar{3}41$	-25.1	$\bar{2}36$	-24.6	$45\bar{3}$	-25.8	$3\bar{5}\bar{3}$	-30.4
001	0	001	0.0	$1\bar{1}0$	0.0	001	0.0	$01\bar{1}$	0.0	$1\bar{1}0$	0.0	001	0.0	$01\bar{1}$	0.0	001	0.0	$\bar{1}11$	0.0	$01\bar{1}$	0.0	$1\bar{1}0$	0.0	$1\bar{1}0$	0.0
017	8.1	$1\bar{1}7$	11.4	$45\bar{1}$	10.9	$1\bar{2}7$	17.7	$13\bar{5}$	17.0	$54\bar{2}$	18.4	$1\bar{3}7$	24.3	$13\bar{6}$	20.2	$23\bar{6}$	31.0	$\bar{3}25$	20.6	$23\bar{6}$	24.6	$45\bar{3}$	25.8	$3\bar{5}\bar{3}$	30.4
016	9.5	$1\bar{1}6$	13.3	$34\bar{1}$	13.9	$1\bar{2}6$	20.4	$12\bar{4}$	22.2	$34\bar{2}$	23.2	$1\bar{3}6$	27.8	$12\bar{5}$	25.4	$23\bar{5}$	35.8	$\bar{2}14$	28.1	$22\bar{5}$	30.5	$34\bar{3}$	31.9	$2\bar{4}3$	38.0
015	11.3	$1\bar{1}5$	15.8	$23\bar{1}$	19.1	$1\bar{2}5$	24.1	$11\bar{3}$	31.5	$23\bar{2}$	31.0	$1\bar{3}5$	32.3	$11\bar{4}$	33.5	$23\bar{4}$	42.0	$\bar{1}37$	34.3	$21\bar{4}$	39.6	$23\bar{3}$	41.1	$1\bar{3}3$	49.5
014	14.0	$1\bar{1}4$	19.5	$35\bar{2}$	23.4	$1\bar{2}4$	29.2	$31\bar{7}$	42.6	$35\bar{4}$	36.9	$1\bar{3}4$	38.4	$10\bar{3}$	47.9	$23\bar{3}$	50.2	$\bar{1}03$	43.1	$20\bar{3}$	54.0	$12\bar{3}$	55.5	$0\bar{2}3$	66.9
027	15.9	$2\bar{2}7$	22.0	$12\bar{1}$	30.0	$1\bar{2}3$	36.7	$10\bar{2}$	50.7	$1\bar{2}2$	45.0	$1\bar{3}3$	46.0	$21\bar{5}$	58.9	$23\bar{2}$	61.0	$\bar{1}15$	56.3	$41\bar{5}$	64.1	$13\bar{6}$	65.3	$1\bar{3}6$	78.0
013	18.4	$1\bar{1}3$	25.3	$25\bar{3}$	36.6	$2\bar{4}5$	41.8	$31\bar{5}$	61.4	$1\bar{3}4$	56.5	$1\bar{4}6$	63.6	$11\bar{2}$	73.2	$23\bar{1}$	74.5	$\bar{1}27$	61.9	$21\bar{2}$	76.4	$01\bar{3}$	77.1	$1\bar{1}3$	90.0
025	21.8	$2\bar{2}5$	29.5	$13\bar{2}$	40.9	$1\bar{2}2$	48.2	$21\bar{3}$	67.8	$3\bar{5}\bar{4}$	74.8	$2\bar{6}3$	64.6	$1\bar{3}1$	72.4	$46\bar{1}$	82.1	$0\bar{1}2$	75.0	$43\bar{3}$	90.0	$1\bar{1}6$	90.0	$3\bar{1}6$	102.0
037	23.2	$1\bar{1}2$	35.2	$14\bar{3}$	46.1	$2\bar{4}3$	56.2	$3\bar{2}4$	74.8	$4\bar{3}5$	78.5	$26\bar{1}$	81.0	$23\bar{3}$	90.0	$23\bar{0}$	90.0	$14\bar{5}$	90.0	$22\bar{1}$	103.6	$\bar{1}03$	102.9		
012	26.6	$3\bar{3}5$	40.1	$15\bar{4}$	49.1	$1\bar{2}1$	65.9	$1\bar{1}1$	90.0	$\bar{1}1\bar{4}$	90.0	$1\bar{3}0$	90.0	$35\bar{4}$	95.7	$46\bar{1}$	97.9	$13\bar{3}$	97.6						
035	31.0	$2\bar{2}3$	43.5	$0\bar{1}1$	60.0	$3\bar{6}2$	73.4	$4\bar{5}\bar{3}$	101.5	$\bar{2}16$	98.6	$26\bar{1}$	99.0					$25\bar{4}$	105.0						
023	33.7	$3\bar{3}4$	46.6	$\bar{1}54$	70.9	$3\bar{6}1$	81.5											$12\bar{1}$	118.1						
034	36.9	$44\bar{5}$	48.5			$1\bar{2}0$	90.0											$45\bar{2}$	127.0						
045	38.7	$1\bar{1}1$	54.7			$36\bar{1}$	98.5											$35\bar{1}$	133.1						
011	45.0	$3\bar{3}2$	63.4															$23\bar{0}$	143.2						
054	51.3	$5\bar{5}3$	67.0															$34\bar{1}$	154.9						
		$22\bar{1}$	70.5															$1\bar{1}1$	180.0						
		$55\bar{2}$	73.9															$3\bar{2}\bar{5}$	200.6						
		$35\bar{1}$	76.7																						
		$44\bar{1}$	80.0																						
		$55\bar{1}$	81.9																						
		$1\bar{1}0$	90.0																						
		$55\bar{1}$	98.1																						

TABLE 12

Angles Between Prominent Planes For a Cubic Crystal

Angle	Plane	Plane	Zone
15.8	$1\bar{1}1$	$2\bar{2}1$	110
17.1	$1\bar{2}2$	$1\bar{2}1$	210
18.4	012	011	100
19.5	$1\bar{1}2$	$1\bar{1}1$	110
24.1	$1\bar{2}1$	$1\bar{2}0$	210
26.6	001	012	100
26.6	$1\bar{2}2$	$0\bar{1}2$	221
27.2	$2\bar{1}\bar{2}$	$2\bar{2}\bar{1}$	322
30.0	$1\bar{1}0$	$1\bar{2}1$	111
33.6	$1\bar{1}2$	$1\bar{2}\bar{1}$	311
35.2	001	$1\bar{1}2$	110
35.3	$1\bar{1}2$	$2\bar{2}1$	110
35.3	$1\bar{1}1$	$1\bar{1}0$	110
36.8	$0\bar{1}2$	$\bar{1}02$	221
39.0	$2\bar{2}1$	$2\bar{2}\bar{1}$	110
39.3	$10\bar{2}$	$1\bar{1}\bar{1}$	211
41.8	$1\bar{2}2$	$1\bar{2}0$	210
43.1	$0\bar{1}2$	$1\bar{2}1$	321
45.0	$1\bar{1}0$	$1\bar{2}2$	221
45.0	001	011	100

where a is the lattice constant, 2.8610 Å for iron, and h, k, and ℓ are the Millerian indices of the plane. The radius in cm. of a spot on the film for a film-specimen distance of 3 cm. is given by

$$r = 3 \tan(180° - 2\theta) \qquad (3)$$

Table 10 was calculated from Eqs. 1 through 3. The radius of each of the intense spots can be measured and the corresponding plane identified from Table 10. By comparing the photograph with a standard projection of the crystal planes, one may be able to identify the other spots and zones. For a final identification the angles between prominent spots in the various zones are measured, using Greninger's chart (17) and these are then matched with the known angles between various planes in given zones from Tables 11 and 12. These tables were calculated using the crystallographic relations given by Barrett (17). It is sometimes helpful to note that a spot which is a four-fold axis of symmetry is due to a {100} plane and one exhibiting a six-fold axis of symmetry is due to a {111} plane. {110} planes give prominent spots with only a two-fold axis of symmetry.

Once the spots on the photograph have been identified, the location of the specimen and X-ray axes can best be determined with the aid of a stereographic net . The angles between the X-ray axis and several planes having normals near it are measured and then the circles corresponding to these angles are drawn about the respective

planes located in a standard projection. The same procedure is repeated to find the specimen axis, using the hyperbolas due to zones lying near the specimen axis.

Measurements of five independent patterns from Specimen III-17 indicated that the errors in locating the specimen axis were about $\frac{1}{2}^{\circ}$ and those in locating the radius through the reference mark were about 1°.

Determination of Active Slip Directions and Planes

A point on the surface of the fatigue specimen loaded in bending is subject to pure alternating axial tension and compression as shown in Appendix IV. As Gough (4) has shown, it is of interest to find out what stresses result in certain planes on the {110} , {112}, and {113} -type planes in the ⟨111⟩-type direction, since he concluded that slip occurs on these planes. The equilibrium condition from the theory of elasticity requires that the stress on the a plane in the b direction, τ_{ab}, is related to the axial stress by the relation

$$\tau_{ab} = l_{a3}\, l_{b3}\, \tau_{33} \,, \tag{4}$$

where the l's denote direction cosines. In other words

$$\tau_{ab} = \cos\theta_a \cos\theta_b \, \tau_{33} \,, \tag{4a}$$

where θ is the polar angle of the plane or direction in

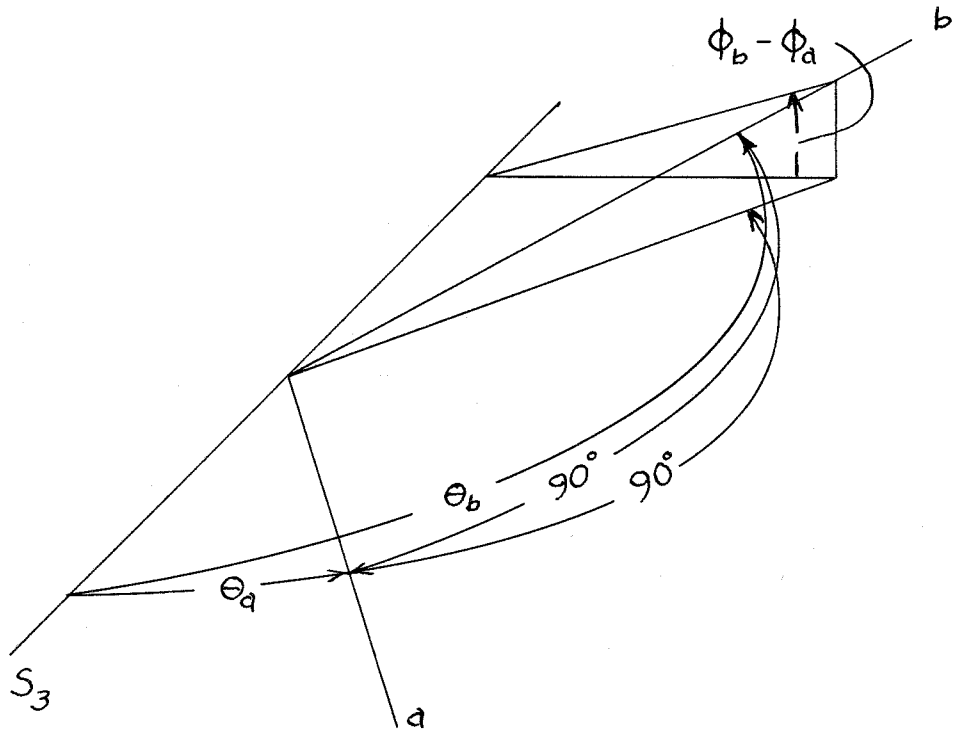

Fig. 55

Condition for the a Plane to Contain the b Direction

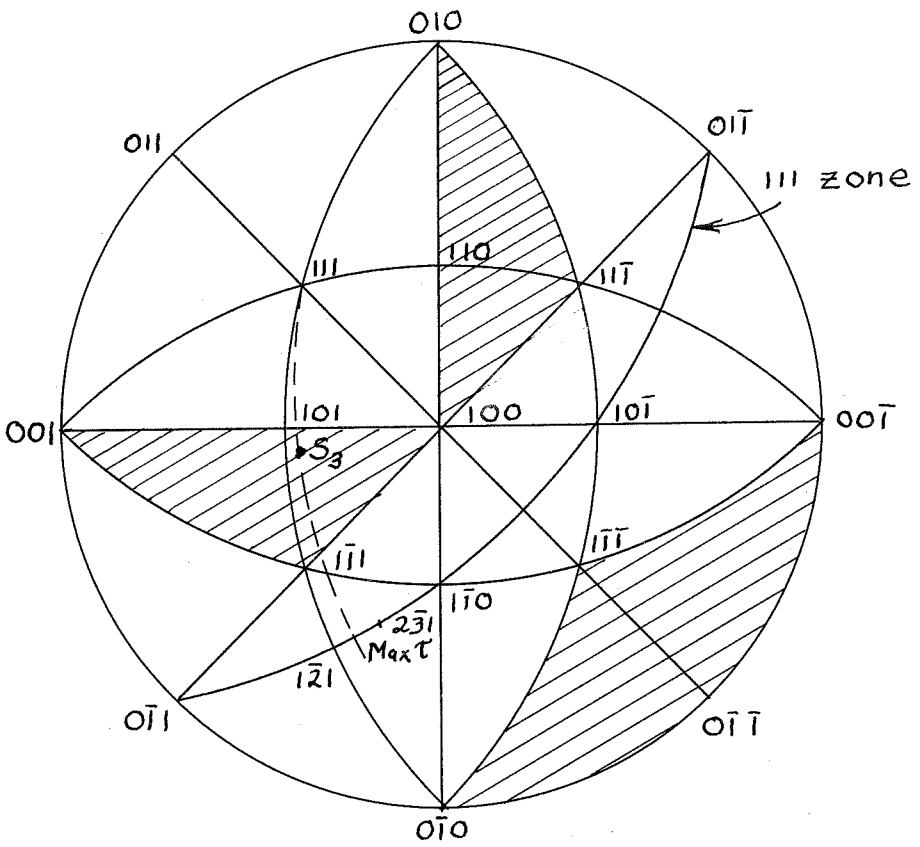

Fig. 56

Planes of Critical Shear Stress

question relative to the specimen axis as shown in Fig. 55. In this figure the b direction is projected onto the plane containing the S_3 and a directions. The condition that the b direction lies in the a plane requires that

$$\cos(\phi_b - \phi_a) = -\frac{\cot \theta_a}{\cot \theta_b} , \tag{5}$$

where ϕ is the meridianal angle of a direction relative to the polar coordinates of the specimen. To find which plane containing a $\langle 111 \rangle$ direction has the maximum shear stress, combine Eqs. 4a and 5, obtaining

$$\tau_{ab} = \frac{\cos \theta_b \quad \tau_{33}}{\sqrt{1 + \cot^2 \theta_b \sec^2(\phi_b - \phi_a)}} . \tag{6}$$

It can be seen that τ_{ab} attains a maximum when $\phi_a = \phi_b$, in which case Eq. 6 reduces to

$$\tau_{ab} = \frac{1}{2} \sin 2\theta_b \quad \tau_{33} . \tag{7}$$

From Eq. 7 the resolved shear stress is a maximum if the 111 direction makes an angle of 45° with the specimen axis, and the stress falls off symmetrically as the angle increases or decreases from that value. In Fig. 56 the shaded regions indicate locations of the specimen axis in which the maximum resolved shear

stress in the $[111]$ direction is greater than in the $[11\bar{1}]$, the $[1\bar{1}\bar{1}]$, or the $[1\bar{1}1]$ directions.

Gough's hypothesis (4) is that slip actually occurs on the $\{110\}$, $\{112\}$, or $\{123\}$ planes. It is of interest to see how much the maximum stress on planes of those types differs from the maximum given by Eq. 7. From Eq. 6 the percent reduction in stress will be the most for the largest value of $\cot^2(\theta_b)$ and $\sec^2(\phi_b - \phi_a)$. Table 11 shows that the largest angle between two $\{110\}$, $\{112\}$, or $\{123\}$ planes containing the same $\langle 111\rangle$ direction (lying in a $\langle 111\rangle$ zone) is 19.1^0 between $\{110\}$ and $\{123\}$ planes. The maximum value for $\phi_b - \phi_a$, then, will be half that, or 9.6^0. From Fig. 56 it can be seen that the minimum value for θ_b occurs when the specimen axis is in the $\langle 110\rangle$ direction, in which case $\theta_b = 35.3^0$ (see Table 11). For this case the maximum deviation of $\phi_b - \phi_a$ from zero results in a decrease of resolved shear stress of only about 1%. Near the boundaries of the shaded regions in Fig. 56 this small difference may be enough to throw the slip from one $\langle 111\rangle$ direction to another. Hence the boundaries are not exact if we assume slip to occur only on the $\{110\}$, $\{112\}$, or $\{123\}$ planes. In practice, once the most likely slip direction is found using Fig. 56, a great circle can be passed through the slip direction and the specimen axis and extended to intersect the zone of planes containing the slip direction. This great circle is the

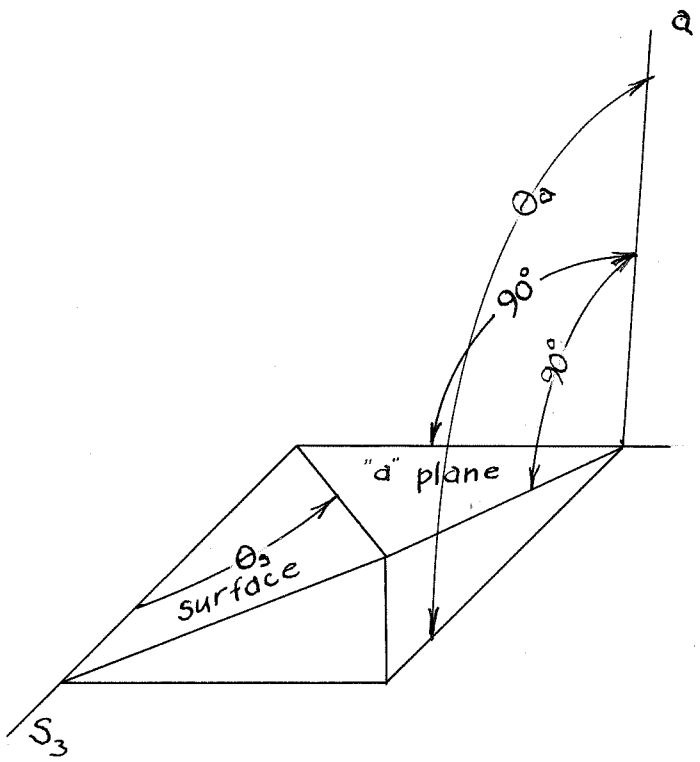

Fig. 57

Trace of plane on specimen surface

locus of planes for which $\phi_b - \phi_a = 0$. According to Gough's hypothesis, (4), the active planes will be those in the zone on either side of the intersection. If the specimen axis lies near one of the boundaries of the shaded regions in Fig. 56, it may be well to calculate the resolved shear stress on the critical planes for the two or three likely slip directions.

Determination of the Trace of the Active Slip

In order to determine whether the calculated slip planes actually were active, their trace in the surface of the specimen can be calculated, and the calculated trace can then be compared with the slip lines observed under the microscope. Fig. 57 illustrates the derivation and symbols of Eq. 8 given by Gough (3):

$$\sin(\phi - \phi_a) = -\frac{\cot \theta_a}{\tan \theta_s} . \qquad (8)$$

APPENDIX IV: DEFORMATION OF ANISOTROPIC BARS IN TENSION, BENDING, and TORSION

Variation of Elastic Constants with Orientation

One important criterion for the method of loading a single crystal fatigue specimen is that the stresses be calculable and that the deformations be ones which can be accomodated by a simple fatigue testing machine. In ordinary fatigue testing, a relatively long specimen of circular cross section is loaded in tension, bending, or torsion. This Appendix treats the stress and deformation of anisotropic materials under these loading systems.

It is convenient to use tensor notation in which the axes of a Cartesian coordinate system are denoted by x_i, where i may take on the value 1, 2, or 3. The stress on the i plane in the j direction is denoted by τ_{ij}, where j, also, may take on the values 1, 2, or 3. By considering the equilibrium of a differential cubic element it can be shown that

$$\tau_{ij} = \tau_{ji} . \tag{1}$$

If u_i is the displacement of a particle in the i direction, then the strain at a point is defined by

$$\varepsilon_{ij} = \frac{1}{2}\left(\frac{\partial u_i}{\partial x_j} + \frac{\partial u_j}{\partial x_i} \right). \tag{2}$$

It follows that

$$\varepsilon_{ij} = \varepsilon_{ji} \tag{3}$$

The strain thus defined is identical to the engineering strain for normal strains, where $i = j$, but for shear strains, where $i \neq j$, this strain is half the engineering strain. It is an experimental observation that the strains are linear functions of the stresses, at least for low stresses. The resulting equation is known as the generalized Hooke's law:

$$\varepsilon_{ij} = S_{ijkl}\, \tau_{kl} . \tag{4}$$

From Eq. 1 and Eq. 3 it follows that

$$S_{ijkl} = S_{jikl} = S_{jilk} = S_{ijlk} . \tag{5}$$

These constants are related to the equations quoted in the literature (17) as follows:

$$\begin{aligned} S_{1111} &= S_{11} \\ S_{1122} &= S_{12} \\ S_{1123} &= \tfrac{1}{2} S_{14} \\ S_{2323} &= \tfrac{1}{4} S_{44} \\ S_{3112} &= \tfrac{1}{4} S_{56} \qquad \text{etc.} \end{aligned} \tag{6}$$

Note that the tensor subscripts 11 are replaced by 1; 22 by 2; 33 by 3; 23 or 32 by 4; 31 or 13 by 5; and 12 or 21 by 6. For a material to be isotropic it is necessary

that (29)

$$S_{1111} = S_{2222} = S_{3333} \quad , \tag{7a}$$

$$S_{1122} = S_{2233} = S_{3311} = S_{1133} \quad \text{etc.,} \tag{7b}$$

$$S_{1212} = S_{2323} = S_{3131} \quad , \tag{7c}$$

$$\text{All others} = 0 \quad , \tag{7d}$$

$$S_{1111} - S_{1122} - 2S_{2323} = 0 \quad . \tag{7e}$$

For a crystal with a cubic structure in which the coordinate axes are parallel to the cube edges, Eqs. 7a through 7d hold but Eq. 7e does not. Since the axis of a single crystal specimen may not be lined up with a cube edge, it is necessary to find out what the elastic constant will be in an arbitrary coordinate system whose stress and strains will be denoted by the subscripts i, j, k, and ℓ. Strains and stresses in the crystallographic coordinate system will be denoted by the subscripts $\alpha, \beta, \gamma,$ and δ.

The elastic constants in the new direction can be found from the stress and strain in the new directions. Denote the direction cosines between the x_α and the x_i axes by $\ell_{\alpha i}$. Then using the summation convention in which any subscripts appearing twice in the same term are summed

over,

$$x_\alpha = \ell_{\alpha i}\, x_i .$$

That is, $$x_\alpha = \ell_{\alpha 1} x_1 + \ell_{\alpha 2} x_2 + \ell_{\alpha 3} x_3 . \qquad (8)$$

The stress on the γ plane in the δ direction is denoted by $\tau_{\gamma\delta}$. Then by considering the equilibrium of a differential tetrahedron formed by the intersection of a plane, γ, with the coordinate planes, k, it is possible to show that stresses in the two coordinate systems are related by

$$\tau_{\gamma\delta} = \ell_{\gamma\kappa}\, \ell_{\delta\ell}\, \tau_{\kappa\ell} . \qquad (9)$$

To find the strain in a new coordinate system, consider that since

$$x_\beta = \ell_{\beta j}\, x_j \quad , \text{and}$$

$$u_i = \ell_{i\alpha}\, u_\alpha ,$$

therefore $$\frac{\partial u_i}{\partial x_j} = \ell_{i\alpha}\, \ell_{j\beta}\, \frac{\partial u_\alpha}{\partial x_\beta}$$

and $$\frac{\partial u_j}{\partial x_i} = \ell_{j\alpha}\, \ell_{i\beta}\, \frac{\partial u_\alpha}{\partial x_\beta} . \qquad (10)$$

On interchanging the indices α and β, which are summed over, Eq. 10 combines with the definition of strain, Eq. 2, to give

$$\varepsilon_{ij} = \ell_{i\alpha}\, \ell_{j\beta}\, \varepsilon_{\alpha\beta} . \qquad (11)$$

Now combining Eqs. 9 and 11 with the assumption of Hooke's law in the crystallographic coordinates, it follows that

$$\varepsilon_{ij} = l_{i\alpha} l_{j\beta} S_{\alpha\beta\gamma\delta} l_{\gamma k} l_{\delta l} \tau_{kl} . \qquad (12)$$

This gives the elastic constant in an arbitrary coordinate system as a function of those in the crystallographic system and the direction cosines:

$$S_{ijkl} = l_{i\alpha} l_{j\beta} l_{k\gamma} l_{l\delta} S_{\alpha\beta\gamma\delta} . \qquad (13)$$

When the material is isotropic so that

$$S_{ijkl} = S_{\alpha\beta\gamma\delta}$$

when $i = \alpha$, $j = \beta$, etc., then

$$S_{1111} - S_{1122} - 2S_{2323} = 0 . \qquad (7e)$$

Therefore it would seem reasonable to look for a simpler expression for the elastic constants in the form

$$S_{ijkl} = S_{\alpha\beta\gamma\delta} + (S_{1111} - S_{1122} - 2 S_{2323}) f(l_{i\alpha}) \qquad (14)$$

where f is some unknown function of the direction cosines. Such a relation was found by evaluating Eq. 13 for the different types of elastic constants:

$$S_{ijkl} = S_{\alpha\beta\gamma\delta} + (S_{1111} - S_{1122} - 2 S_{2323}) \left(\sum_{\varepsilon=1}^{3} l_{\varepsilon i} l_{\varepsilon j} l_{\varepsilon k} l_{\varepsilon l} - \delta_{\alpha\beta} \delta_{\beta\gamma} \delta_{\gamma\delta} \right) . \qquad (15)$$

Here $i = \alpha$, $j = \beta$, etc. and $\delta_{\alpha\beta}$ is the Kronecker δ whose value is unity when the subscripts are equal, and zero otherwise. This expression agrees with special cases given in the literature (2), (29), except for one equation of Voigt's ((29), p. 593, line 4). His equation is probably in error, however, for it does not reduce to an identity for zero rotation.

For fatigue testing of single crystals it will be seen below that the elastic constant S_{3331} causes the most marked effects due to anisotropy. The maximum value which this constant attains for iron will now be found. From Eq. 15

$$S_{3331} = (S_{1111} - S_{1122} - 2S_{2323})(l_{13}^3 l_{11} + l_{23}^3 l_{21} + l_{33}^3 l_{31}). \quad (16)$$

The right-hand factor can be thought of as the dot product of the unit vector $\bar{l}_1$ with components l_{11} , l_{21} , and l_{31} , with a vector whose components are l_{13}^3 , l_{23}^3, and l_{33}^3 , which will be called $\overline{l_3^3}$. Since $\bar{l}_1$ and $\bar{l}_3$ are orthogonal, this dot product will be zero when $\bar{l}_1$ is perpendicular to the plane of $\bar{l}_3$ and $\overline{l_3^3}$, and will be an extremum only if $\bar{l}_1$ is in the plane of the other two, as shown in Fig. 58.

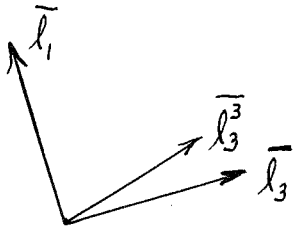

Fig. 58

If $\bar{l}_1$ does lie in this plane, then since $\bar{l}_1$ and $\bar{l}_3$ are unit vectors, the dot product $\bar{l}_1 \cdot \bar{l}_3$ will be equal in magnitude to the vector product $\bar{l}_3 \times \bar{l}_3$. When this vector product is dotted into itself, expressed in terms of the components l_{13} , l_{23} , and l_{33} , and reduced to a function of two variables by the relation $l_{33}^2 = 1 - l_{13}^2 - l_{23}^2$, it becomes

$$\begin{aligned} f^2(l_{13}, l_{23}) = & -4l_{13}^8 - 8l_{13}^6 l_{23}^2 - 12 l_{13}^4 l_{23}^4 - 8 l_{13}^2 l_{23}^6 - 4 l_{23}^8 \\ & + 8 l_{13}^6 + 13 l_{13}^4 l_{23}^2 + 13 l_{13}^2 l_{23}^4 + 8 l_{23}^6 \\ & - 5 l_{13}^4 - 6 l_{13}^2 l_{23}^2 - 5 l_{23}^4 \\ & + l_{13}^2 + l_{23}^2 . \end{aligned} \tag{17}$$

Because of the symmetry of a cubic crystal, this function need only be considered over the region $0 \leq l_{13} \leq 0.5$, $0 \leq l_{23} \leq l_{13}$. A plot of the function over this region indicates that the maximum is attained along the line $l_{13} = l_{23}$. Along this line, the maximum occurs at

$$l_{13} = l_{23} = \sqrt{\frac{13 - \sqrt{13}}{48}} = .3047 . \tag{18}$$

The corresponding value of $l_{13}^3 l_{11} + l_{23}^3 l_{21} + l_{33}^3 l_{31}$ is 0.296. For iron the following values for the elastic constant were obtained by Kimura and Ohno (2):

$$S_{1111} = 52.8 \times 10^{-9} \text{ in.}^2/\text{lb.}$$
$$S_{1122} = -19.9 \times 10^{-9} \text{ in.}^2/\text{lb.}$$
$$S_{2323} = 15.4 \times 10^{-9} \text{ in.}^2/\text{lb.}$$
$$\left(S_{1111} - S_{1122} - 2S_{2323}\right) = 41.8 \times 10^{-9} \text{ in.}^2/\text{lb.}$$

The corresponding values for S_{3331} and S_{3333} at the orientation for which S_{3331} is a maximum are

$$S_{3331} = 12.4 \times 10^{-9} \text{ in}^2/\text{lb.}$$
$$S_{3333} = 45.8 \times 10^{-9} \text{ in}^2/\text{lb.}$$

Deformations of Circular Anisotropic Bars

The solutions for tension, bending, and torsion of anisotropic bars have been worked out by Voight (29), and the torsion solution was also given by Wright (30). If the distribution is linear in the isotropic case, then the same stress distribution holds in the anisotropic case. The resultant deformations are given below under the boundary conditions that the slope and deflection of the specimen axis are zero at the origin of coordinates.

Deformation Due to Axial Tension

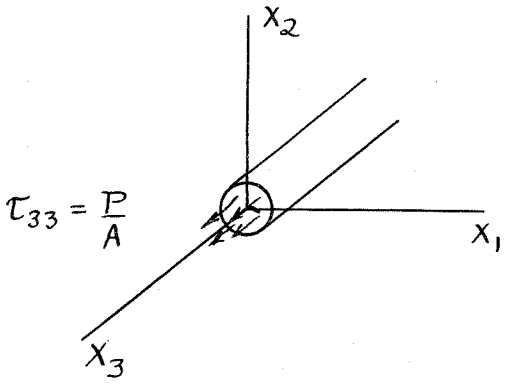

Fig. 59

With the coordinate system and loading given in Fig. 59, the displacements u_1, u_2, and u_3 in the x_1, x_2, and x_3 directions are given by

$$u_1 \frac{A}{P} = S_{1133} x_1 + S_{1233} x_2$$

$$u_2 \frac{A}{P} = S_{1233} x_1 + S_{2233} x_2 \qquad (19)$$

$$u_3 \frac{A}{P} = 2 S_{1333} x_1 + 2 S_{2333} x_2 + S_{3333} x_3$$

These equations indicate that a cross section will shear by an amount S_{1233} and be tipped relative to the x_3 axis due to the S_{1333} and S_{2333} terms. If the bar is loaded by

clamping it in grips or by pulling on an enlarged section, the restraint of this tipping will require a bending moment and shear. The bending moment could be avoided only if the grips or enlarged ends pivot near the beginning of the narrowed down section. A special machine would therefore be required for repeated axial stress tests on single crystals.

Deformation Due to Pure Bending

For pure bending about the x_1 axis, the stress distribution is given by

$$\tau_{33} = \frac{M x_2}{I} \tag{20}$$

where M is the applied bending moment and I the moment of inertia about the neutral axis. This leads to the following expressions for the displacements:

$$u_1 \frac{I}{M} = \underline{S_{1133}\, x_2 x_1} + S_{1233}\, x_2^2 + S_{3133}\, x_2 x_3$$

$$u_2 \frac{I}{M} = \underline{S_{2233}\, \frac{x_2^2}{2}} - \underline{S_{3333}\, \frac{x_3^2}{2}} - S_{3133}\, x_1 x_3 - \underline{S_{1133}\, \frac{x_1^2}{2}} \tag{21}$$

$$u_3 \frac{I}{M} = \underline{S_{3333}\, x_2 x_3} + S_{3133}\, x_1 x_2 + S_{2333}\, x_2^2 ,$$

The underlined terms are the ones present in the isotropic case. The effect of anisotropy, then, is to dish the sides (due to the S_{1233} terms in the expression for u_1); to dish the ends around the x_1 axis (due to the S_{2333} term in the expression for u_3); to distort the cross section by moving one pair of diagonals forward and the other pair backwards (due to the S_{3133} term in the expression for u_3), and to produce a twist (due to the S_{3133} terms in the expressions for u_3). The most important result is that there is no elastic constant affecting the overall lateral deformation except S_{3333}. In a rotating beam fatigue test, therefore, any change in lateral deflection and resultant vibration in the machine as the specimen rotates would be due to a change in S_{3333}. That constant is invariant with respect to rotation about the x_3 axis, however, so there will be no lateral vibration of the machine due to anisotropy.

The angle of twist per unit length is given by

$$\frac{\partial \theta}{\partial x_3} = \frac{\partial}{\partial x_3}\left(\frac{\partial u_2}{\partial x_3} - \frac{\partial u_1}{\partial x_2}\right) = -\frac{2\, S_{3133}\, M}{I} \quad . \tag{22}$$

The factor S_{3133} is not invariant with respect to rotation about the three axes so there will be a torsional oscillation due to the anisotropy. As found above, however, the maximum value of S_{3133} is 12.4 $\times 10^{-9}$ in.^{2}/lb. The resulting torsional oscillations for the specimens and machine used in these tests cause stresses of less than 100 psi.

Deformation Due to Pure Torsion

In rectangular coordinates the stress is given by

$$\tau_{31} = -\frac{T x_2}{I_p}$$
$$\tau_{32} = \frac{T x_1}{I_p} , \qquad (23)$$

where I_p is the polar moment of inertia and T the applied torque. These stresses cause the following displacements:

$$\frac{u_1 I_p}{T} = S_{1123} x_1^2 - 2S_{1131} x_1 x_2 - (S_{2223} + 2S_{1231}) x_2^2 - \underline{2(S_{2323} + S_{3131}) x_2 x_3} - S_{3323} x_3^2$$

$$\frac{u_2 I_p}{T} = 2S_{2223} x_1 x_2 - S_{2231} x_2^2 + S_{3331} x_3^2 + \underline{2(S_{2323} + S_{3131}) x_3 x_1} + (S_{1131} + 2S_{1223}) x_1^2$$

$$\frac{u_3 I_p}{T} = 2S_{3323} x_1 x_3 - 2S_{3331} x_2 x_3 + 2S_{3123} x_1^2 + 2(S_{2323} - S_{3131}) x_1 x_2 - 2S_{2331} x_2^2 . \qquad (24)$$

The underlined terms are those present in the isotropic case. It is evident that the anisotropy leads to a very complicated deformation, an important feature of which is the bending of the specimen axis due to the S_{3323} and S_{3331} terms in the expressions for u_1 and u_2 respectively.

If the fatigue machine prevents bending of a circular bar in the u_2 direction, for example, then a moment must be applied to straighten out the deformation:

$$\frac{T S_{3331}}{I_p} x_3^2 = u_2 = -\frac{S_{3333} M x_3^2}{2 I} \qquad (25)$$

Since $\tau_{33} = \frac{M x_2}{I}$ and $\tau_{31} = -\frac{T x_2}{I_p}$,

$$\frac{\tau_{33}}{\tau_{31}} = -\frac{M I_p}{I T} = \frac{2 S_{3331}}{S_{3333}} \qquad (26)$$

As shown on p. 122, this ratio can amount to 0.54. Therefore in any torsion fatigue machine for single crystals either bending restraints must be avoided, or the resulting bending stress must be calculated and reported.

REFERENCES

(1) L. H. Donnell, "Stress Concentrations Due to Elliptical Discontinuities in Plates Under Edge Forces," Karman Anniversary Volume, (1941), California Institute of Technology.

(2) R. Kimura and K. Ohno, "On the Elastic Constants of Single Crystals of Iron", Tohoku Imperial University Science Reports, (1934), First Series, v. 23, p. 359.

(3) H. J. Gough, "The Behavior of a Single Crystal of α Iron Subjected to Alternating Torsional Stresses", Proceedings of the Royal Society of London, Series A, (1928), v. 118, p. 498.

(4) H. J. Gough, "Crystalline Structure in Relation to Failure of Metals, Especially by Fatigue", Proceedings of the American Society for Testing Materials, (1933), v. 33, p. 3.

(5) G. I. Taylor and C. F. Elam, "Distortion of Iron Crystals", Proceedings of the Royal Society of London, Series A, (1926), v. 112, p. 337.

(6) E. S. Barrett, G. Ansel, and R. F. Mehl, "Slip, Twinning, and Cleavage in Iron and Silicon Ferrite", Transactions of the American Society for Metals, (1937), v. 25, p. 702.

(7) E. F. Elam, "The Distortion of β Brass and Iron Crystals", Proceedings of the Royal Society of London, Series A, (1936), v. 153, p. 193.

(8) J. A. Ewing and J. C. W. Humphrey, "The Fracture of Metals Under Repeated Alternations of Stress", Philosophical Transactions of the Royal Society, Series A, (1903), v. 200, p. 241.

(9) T. F. Stanton and L. Bairstow, "On the Resistance of Iron and Steel to Reversals of Direct Stress", Proceedings of the Institution of Civil Engineers, (1906), v. 166, p. 78.

(10) H. J. Gough and D. Hanson, "Behavior of Metals Subjected to Repeated Stresses", Proceedings of the Royal Society of London, Series A, (1923), v. 104, p. 538.

(11) F. F. Lucas, "Observations on the Microstructure of the Path of Fatigue Failure in a Specimen of Armco Iron", Transactions of the American Society of Steel Treating, (April, 1927), v. xi, No. 4, p. 531.

(12) H. F. Moore and T. Ver, "A Study of Slip Lines, Strain Lines, and Cracks in Metals Under Repeated Stress," University of Illinois Engineering Experiment Station Bulletin 208, (1930).

(13) L. B. Pfeil, "The Deformation of Iron, with Particular Reference to Single Crystals", Iron and Steel Institute, Carnegie Scholarship Memoirs, (1926), v. XV, p. 319.

(14) H. F. Moore and J. B. Kommers, "An Investigation of the Fatigue of Metals", University of Illinois Engineering Experiment Station Bulletin 124,(1921).

(14a) J. B. Kommers, "The Effect of Understressing on Cast Iron and Open Hearth Iron", Proceedings of the American Society for Testing Materials,(1930), v. 30, p. 368.

(15) B. Epstein, "Aspects of the Fracture Problem", Journal of Applied Physics, (Feb. 1948), v. 19 #2, p. 140.

(16) Battelle Memorial Institute, Prevention of the Failure of Metals Under Repeated Stress, Wiley& Sons, New York, (1941).

(17) C. S. Barrett, Structure of Metals, McGraw Hill, New York, (1943).

(18) K. M. Greenland, "Slip Bands in Mercury Single Crystals", Proceedings of the Royal Society of London, Series A, (1937), v. 163, p. 34.

(19) P. G. Hoel, Introduction to Mathematical Statistics, Wiley & Sons, New York, (1947).

(20) H. F. Moore and T. M. Jasper, "An Investigation of the Fatigue of Metals", University of Illinois Engineering Experiment Station Bulletin 142, (1924), p.1.

(21) R. L. Kenyon and R. F. Mehl, "The Effects of Cold Work on the Properties of Iron", Metals Handbook, (1948), p. 438.

(22) H. B. Dwight, Tables of Integrals and Other Mathematical Data, Macmillan, New York, (1947)

(23) R. V. Southwell and H. J. Gough, "The Concentration of Stress in the Neighborhood of a Small Spherical Flaw; and the Propagation of Fatigue Fractures in Statistically Isotropic Materials", Philosophical Magazine, (1926), Series VII, v.1, p. 71.

(24) A. Dahl, "Temperature: Its Measure and Control in Science and Industry", American Institute of Physics, (1941), p. 1247.

(25) N. A. Ziegler, "Production and Some Properties of Large Iron Crystals", Transactions of the Iron and Steel Division of the American Institute of Mining and Metallurgical Engineers, (1930), v.90, p. 209.

(26) C. A. Edwards and L. B. Pfeil, "The Tensile Properties of Single Iron Crystals and the Influence of Crystal Size Upon the Tensile Properties of Iron", Journal of the Iron and Steel Institute, (1925), v. 112, p. 79.

(27) C. A. Edwards and L. B. Pfeil, "The Production of Large Crystals by Annealing Strained Iron," Journal of the Iron and Steel Institute, (19), v. 109, p. 129.

(28) F. Adcock and C. A. Bristow, "Iron of High Purity", Proceedings of the Royal Society of London, Series A, (1936), v. 153, p. 172.

(29) W. Voight, Lehrbuch der Kristallphysik, 2nd Edit., Leipzig, (1928).

(30) S. J. Wright, "The Torsion of Circular and Elliptical Cylinders of Homogeneous Aeolotropic Materials", Royal Aeronautical Establishment Reports and Memoranda, No. 1031 (1926).